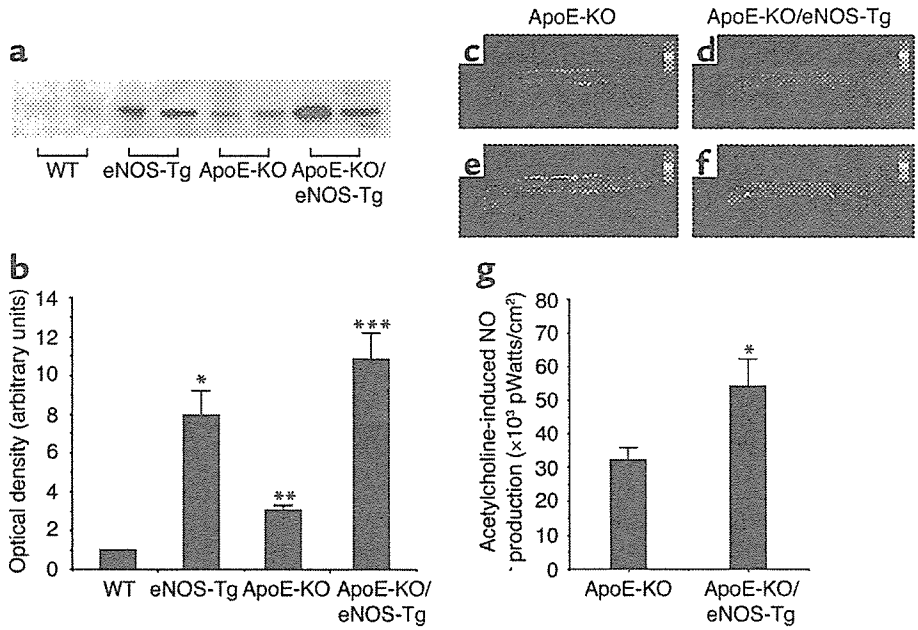

Figure 4

Expression of eNOS and NO production in aortas. (**a**) Immunoblot analysis for eNOS in aortas. Expression of eNOS in aortas from eNOS-Tg and apoE-KO/eNOS-Tg mice was significantly higher than that in WT mice. Note that the protein levels in aortas from apoE-KO mice or apoE-KO/eNOS-Tg mice were not reduced compared with WT mice or eNOS-Tg mice, respectively, but rather increased in the early phase of atherosclerosis. (**b**) Immunoblots were analyzed and quantified by densitometry. $n = 6$ for each group. $^*P < 0.001$ vs. WT mice; $^{**}P < 0.05$ vs. WT mice; $^{***}P < 0.01$ vs. apoE-KO mice. (**c–g**) NO production in aortas was evaluated by fluorescence detection with DAF-2 DA as described in Methods. (**c–f**) Shown are representative photographs of the detected NO production in aortas from apoE-KO (**c** and **e**) and apoE-KO/eNOS-Tg mice (**d** and **f**) before (**c** and **d**) and after (**e** and **f**) incubation with acetylcholine (1 μmol/l). NO production was clearly visualized by administration of acetylcholine (**e** and **f**). (**g**) Quantitative analysis showed that endothelium-derived NO production in apoE-KO/eNOS-Tg mice was significantly higher than that in apoE-KO mice. Acetylcholine-stimulated NO production was expressed as picowatts per centimeter square. $n = 6$ for each group. $^*P < 0.05$ vs. apoE-KO mice.

plaque lesions of apoE-KO mice (Figure 5, b and e). In apoE-KO/eNOS-Tg mice, MCLA signal was intensely visualized and more extensively distributed from the aortic arch to the iliac bifurcation (Figure 5, c and f).

Quantitative analysis showed that superoxide production in nonplaque areas was increased 3.3-fold in apoE-KO/eNOS-Tg mice and 2.1-fold in apoE-KO mice compared with normal aortic vessels in WT mice (Figure 5g). In plaque areas, superoxide generation was further increased more than tenfold in both apoE-KO and apoE-KO/eNOS-Tg mice compared with WT mice. However, the increase in superoxide production was more significantly augmented in both areas of apoE-KO/eNOS-Tg mice compared with those of apoE-KO mice.

To examine the source of superoxide generation in aortas, the endothelium was sequentially removed. In apoE-KO mice, the endothelial denudation resulted in only slight reduction of superoxide production in both plaque and nonplaque areas (Figure 5h). In contrast, superoxide levels in nonplaque areas in apoE-KO/eNOS-Tg mice were significantly decreased by the endothelial denudation, showing that the vascular endothelium is the pivotal source of superoxide generation in aortas of apoE-KO/eNOS-Tg mice.

Reduced BH_4 contents in atherosclerotic vessels. Enhanced superoxide production and decreased NO bioactivity in the endothelium raised a possibility that activation of eNOS might be dysregulated under hypercholesterolemia in our model. Previous studies demonstrated that loss or insufficiency of BH_4, an essential cofactor of NOS, impaired the physiological function of NOS in vitro or in vivo (18, 30, 31). Therefore, we subsequently measured tissue biopterin contents in aortas to examine the roles of BH_4 on the atherogenesis. In apoE-KO mice, BH_4 contents in aortas were approximately 50% decreased compared with WT mice (WT: 5.13 ± 0.01 pmol/mg protein; apoE-KO: 2.56 ± 0.01 pmol/mg protein; $P < 0.01$). BH_4 contents in apoE-KO/eNOS-Tg mice were also significantly lower than those in WT mice (apoE-KO/eNOS-Tg: 2.48 ± 0.01 pmol/mg protein), whereas these BH_4 levels in aortas did not differ between apoE-KO and apoE-KO/eNOS-Tg mice. This finding indicates that dysfunctional eNOS was more abundantly present in aortas of apoE-KO/eNOS-Tg mice.

Effects of BH_4 on the development of atherosclerosis in apoE-KO/eNOS-Tg mice. We hypothesized that supplementation of BH_4 could inhibit the progression of atherosclerosis by restoring eNOS function in apoE-KO/eNOS-Tg mice. After 12 weeks of administration, BH_4 treatment significantly reduced the lesion size in the aortic tree by 26% in male and by 28% in female apoE-KO/eNOS-Tg

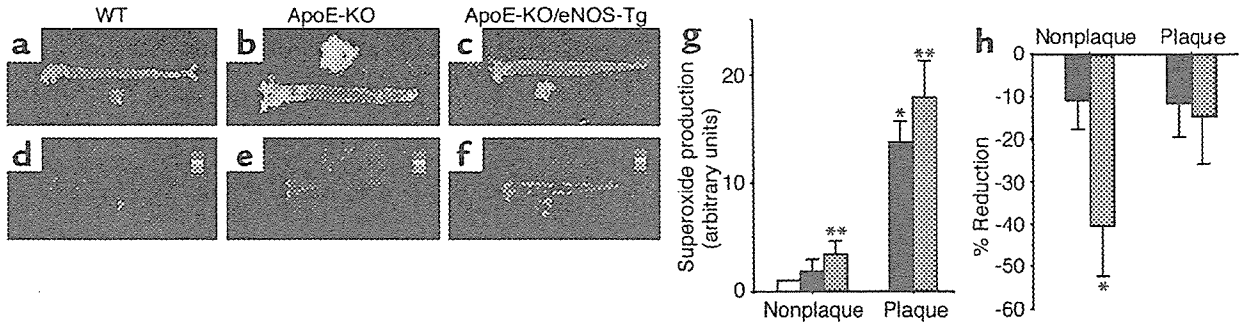

Figure 5
In situ superoxide detection with MCLA in aortas. Shown are representative photographs for chemiluminescent signal of MCLA (**d**–**f**) and each corresponding aorta (**a**–**c**) that was stained with Sudan III from WT mice (**a** and **d**), apoE-KO mice (**b** and **e**), and apoE-KO/eNOS-Tg mice (**c** and **f**). The chemiluminescent signal due to superoxide production was more widely distributed and more strongly visualized in apoE-KO/eNOS-Tg mice compared with apoE-KO mice. (**g**) Quantitative analysis for superoxide levels in nonplaque and plaque areas in WT mice (white bar), apoE-KO mice (black bars), and apoE-KO/eNOS-Tg mice (gray bars). Superoxide levels were expressed as the ratio (fold increase) to the control values obtained from the normal aortic vessels of WT mice. Superoxide production in apoE-KO/eNOS-Tg mice was significantly increased in both nonplaque and plaque areas compared with apoE-KO mice. n = 6–10 for each group. $^*P < 0.05$ vs. normal vessels in WT mice; $^{**}P < 0.05$ vs. nonplaque areas in apoE-KO mice; $^{***}P < 0.01$ vs. plaque areas in apoE-KO mice. (**h**) Reduction of superoxide levels by endothelial denudation in nonplaque and plaque areas of apoE-KO mice (black bars) and apoE-KO/eNOS-Tg mice (gray bars). Shown is the percentage of decreased superoxide production from each predenuded level. In apoE-KO/eNOS-Tg mice, removal of the endothelium resulted in significantly marked decreases in superoxide production in nonplaque areas of the vessels. n = 5–6 for each group. $^*P < 0.01$ vs. nonplaque areas in apoE-KO mice.

mice (Figure 6c). In apoE-KO females, the aortic tree lesion size was also decreased by BH_4 treatment compared with untreated females (Figure 6d); however, the degree of the reduction size was comparatively smaller than in apoE-KO/eNOS-Tg mice. In contrast, apoE-KO males did not show a significant change in the lesion size under BH_4 treatment ($P = 0.25$ vs. untreated males). Plasma lipid profiles were not affected by BH_4 administration at 8 or 12 weeks of treatment (data not shown).

Beneficial effects of BH_4 on the generation of superoxide and NO in the endothelium. Subsequently, the biochemical effects of BH_4 on the production of superoxide and NO were examined in BH_4-treated apoE-KO/eNOS-Tg mice. As shown in Figure 7a, superoxide generation in plaque areas was markedly decreased by BH_4 administration (Figure 7a). Superoxide production in nonplaque areas was also slightly decreased by BH_4 treatment, although the reduction did not reach statistical significance ($P = 0.51$). Endothelial removal decreased superoxide levels in aortas from either BH_4-treated or untreated apoE-KO/eNOS-Tg mice (Figure 7b). However, the degree of the reduction was attenuated by BH_4 treatment. These findings show that supplementation of BH_4 reduced superoxide production in the endothelium. In addition, acetylcholine-stimulated NO production was significantly increased by BH_4 administration (Figure 7c). Thus, the supplementation of BH_4 decreased superoxide generation and increased NO production in the endothelium of apoE-KO/eNOS-Tg mice.

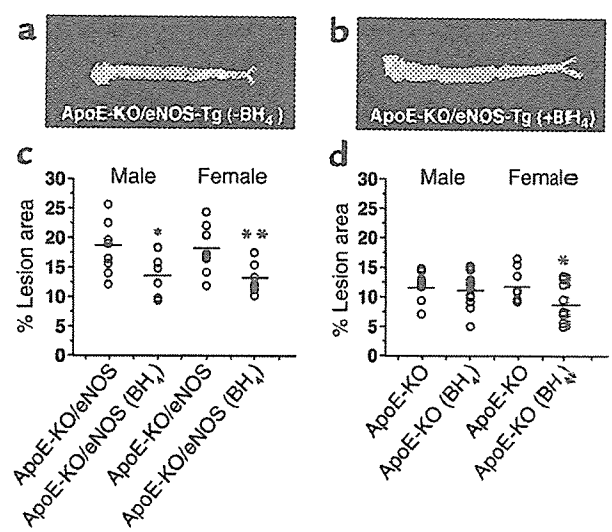

Figure 6
BH_4 suppresses atherosclerotic progression in apoE-KO/eNOS-Tg mice. Representative photographs of Sudan III–stained, longitudinally opened aortas from BH_4-treated (**b**) and untreated (**a**) apoE-KO/eNOS-Tg mice on a high-cholesterol diet for 12 weeks. Atherosclerotic lesion formation was remarkably suppressed by BH_4 administration in apoE-KO/eNOS-Tg mice. (**c**) Quantitative analysis of atherosclerotic lesion size in aortas from apoE-KO/eNOS-Tg mice. In BH_4-treated apoE-KO/eNOS-Tg mice, atherosclerotic lesion size was significantly smaller than in untreated mice. $^*P < 0.05$ vs. untreated apoE-KO/eNOS-Tg males; $^{**}P < 0.01$ vs. untreated apoE-KO/eNOS-Tg females. (**d**) Quantitative analysis of atherosclerotic lesion size in aortas from apoE-KO mice. BH_4 treatment also decreased atherosclerotic lesion size in apoE-KO females; however, the reduction was comparatively smaller than in apoE-KO/eNOS-Tg mice. ApoE-KO males did not show a significant reduction of lesion size. $^*P < 0.05$ vs. untreated apoE-KO females.

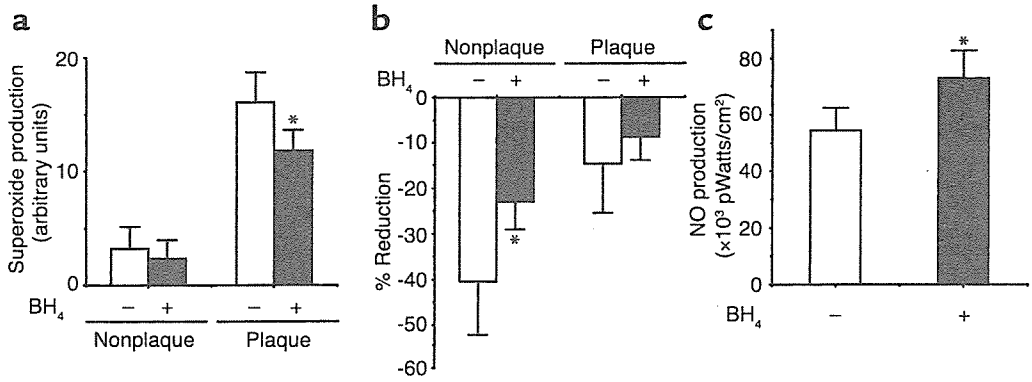

Figure 7

Reduced superoxide production and increased NO production in aortas by BH_4 supplementation in apoE-KO/eNOS-Tg mice. (**a**) Quantitative analysis of superoxide production in both nonplaque and plaque areas in BH_4-treated (black bars) and untreated apoE-KO/eNOS-Tg mice (white bars). BH_4 administration significantly decreased superoxide production in plaque areas in apoE-KO/eNOS-Tg. $n = 6$–10 for each group. $^*P < 0.01$ vs. plaque areas in untreated apoE-KO/eNOS-Tg mice. (**b**) Effects of BH_4 on the superoxide production in the endothelium. Removal of the endothelium reduced superoxide levels in both nonplaque and plaque areas; however, the degree of the reduction was significantly attenuated in nonplaque areas by BH_4 treatment. $^*P < 0.05$ vs. nonplaque areas in untreated apoE-KO/eNOS-Tg mice. (**c**) Effects of BH_4 on NO production in aortas. Acetylcholine-stimulated NO production was significantly increased by BH_4 supplementation in apoE-KO/eNOS-Tg mice. $n = 6$ for both groups. $^*P < 0.05$ vs. untreated apoE-KO/eNOS-Tg mice.

Discussion

The roles of eNOS on the development of atherosclerosis have been vigorously investigated. Previous studies reported that eNOS expression was decreased in the severe atherosclerotic lesions in arteries (32, 33). Recent studies also showed that eNOS deficiency augmented atherosclerotic lesion formation in apoE-KO mice (34, 35). These studies suggest that eNOS acts as an antiatherogenic factor on the vessel walls and that the reduced expression of eNOS precedes more advanced lesion formation of atherosclerosis. Therefore, upregulation of eNOS at the vessel walls has been expected to inhibit the development of atherosclerosis. However, our present study demonstrated that overexpression of eNOS in the endothelium did not inhibit, but accelerated, atherosclerosis in apoE-KO mice.

In the present study, we observed much greater expression of eNOS protein in aortas from apoE-KO/eNOS-Tg mice than in apoE-KO mice (Figure 4, a and b). However, the amount of NO production relative to the eNOS expression level was much lower in apoE-KO/eNOS-Tg mice (Figure 4, c and d). This finding suggests that there exists dysfunction of overexpressed eNOS, which leads to the decrease in NO bioactivity. In accordance with our present results, it was reported that eNOS expression was maintained or even increased in hypercholesterolemic or atherosclerotic vessels (29, 36, 37). These studies raise a possibility that the impaired NO bioactivity, rather than eNOS expression, plays an important role in the initiation or progression of atherosclerosis.

Reactive oxygen species generated by a variety of cells existing in the atherosclerotic vessels are profoundly implicated in the pathogenesis of atherosclerosis (38). Superoxide is one of the strongest oxidants and plays a central role as the source of many reactive oxygen species. Therefore, we next examined the superoxide production in aortas of apoE-KO/eNOS-Tg mice. As shown in Figure 5, the superoxide production in apoE-KO/eNOS-Tg mice was more extensively distributed and significantly increased not only in the atherosclerotic plaque, but also in nonplaque areas, as compared with apoE-KO mice. Removal of the endothelium significantly decreased superoxide production in nonplaque areas in apoE-KO/eNOS-Tg mice, revealing that the endothelium is a major source of superoxide generation in apoE-KO/eNOS-Tg mice. In contrast, the production of NO that is capable of scavenging superoxide was also increased in apoE-KO/eNOS-Tg mice (Figure 4). Therefore, the increases in superoxide generation from the endothelium in apoE-KO/eNOS-Tg mice do not seem to result from the reduced production of NO.

In addition to many potential sources of superoxide in the endothelium, such as NADH/NADPH oxidase, xanthine oxidase, and cyclooxygenase (39), NOS has a potency to produce superoxide rather than NO under the conditions in which its substrate L-arginine or cofactors such as BH_4 are absent (10, 11). It is indicated that lack of or insufficiency of BH_4 relative to the eNOS protein amount is responsible for the impaired endothelial function and superoxide production (40, 41). Therefore, as a mechanism of the accelerated atherosclerosis in apoE-KO/eNOS-Tg mice, we explored a possibility that eNOS dysfunction is due to the relative insufficiency of intracellular BH_4 levels. Indeed, we found that BH_4 contents in aortas were significantly reduced in both apoE-KO and apoE-KO/eNOS-Tg mice compared with those in WT mice. Supplemental BH_4 decreased superoxide production in the endothelium of both plaque and nonplaque areas (Figure 7, a and b) and dramatically reduced the size of atherosclerotic lesions in apoE-KO/eNOS-Tg mice (Figure 6c).

Furthermore, NO production in the endothelium was also significantly increased by BH_4 treatment (Figure 7c). Because BH_4 is proposed as an antioxidant factor at high doses (42), the reduced atherosclerotic lesion by BH_4 treatment might be caused by its antioxidant action. However, the extent of the reduced lesion size was much smaller in BH_4-treated apoE-KO mice than BH_4-treated apoE-KO/eNOS-Tg mice (Figure 6, c and d). Therefore, the inhibitory effects of BH_4 on the atherosclerotic development were much greater in the presence of eNOS overexpression. This observation suggests that the restoration of eNOS function by BH_4 rather than its antioxidant action is mainly responsible for the amelioration of atherosclerotic development. On the other hand, L-arginine is also an essential determinant for NOS activity. It is proposed that its deficiency also causes vascular endothelial dysfunction via a decrease in NO production (43). Although we have not examined the effects of L-arginine treatment on atherogenesis, the possibility can not be excluded that L-arginine also inhibits atherosclerotic progression in apoE-KO/eNOS-Tg mice. Thus, accelerated atherosclerosis by the overexpression of eNOS in apoE-KO mice is at least partly caused by superoxide production from the endothelium through eNOS dysfunction.

Inducible NOS (iNOS) is also shown to be involved in atherogenesis (21, 44, 45). In immunohistochemistry, we detected iNOS expression mainly in the foam cell-rich regions of atherosclerotic lesions in both apoE-KO and apoE-KO/eNOS-Tg mice. However, the expression of iNOS was not obviously different between the two genotypes (data not shown). In accordance with our findings, Niu et al. reported that the depletion of iNOS did not affect the susceptibility to atherosclerosis in mice (44). In contrast, it was also demonstrated that iNOS accelerated lesion formation from the early phase of atherosclerosis and that tissue injury mediated by iNOS progressed along with lesion formation (21, 45). This inconsistency might be due partly to the diversity of atherogenic models; however, the roles of iNOS in atherogenesis might become greater over time with the progression of atherosclerosis. Because the present study was conducted in the relatively early stage of atherosclerosis, the roles of iNOS could be comparatively smaller than the effects of overexpressed eNOS.

Thus, we investigated chronic effects of eNOS overexpression on the development of atherosclerosis using genetically engineered apoE-KO/eNOS-Tg mice. Evidence demonstrates that overexpression of eNOS in the endothelium promoted atherosclerosis in apoE-KO mice. Dysfunction of eNOS that is manifested by the reduced production of NO and increased generation of superoxide in the endothelium seems to be responsible for the progression of atherosclerosis in apoE-KO/eNOS-Tg mice. Furthermore, insufficiency of NOS cofactor BH_4 appears to be involved mainly in the eNOS dysfunction. Our study indicates that eNOS function rather than eNOS protein expression is crucial for the maintenance or the increase of NO bioactivity. Our present findings also provide insight that modulation of NOS cofactors, including BH_4, a major regulator of eNOS, might be a new strategy for the prevention or inhibition of atherosclerosis.

Acknowledgments

This work was partly supported by the Ministry of Education, Culture, Sports, Science, and Technology of Japan (No. 12470154). The authors thank Shun Ishibashi (Department of Endocrinology and Metabolism, Jichi Medical School) for providing us with apoE-KO mice. We are grateful to Kiyoko Matsui and Ikuyo Kitagawa for experimental assistance.

1. Verbeuren, T.J., et al. 1986. Effect of hypercholesterolemia on vascular reactivity in the rabbit. I. Endothelium-dependent and endothelium-independent contractions and relaxations in isolated arteries of control and hypercholesterolemic rabbits. *Circ. Res.* **58**:552–564.
2. Cooke, J.P., et al. 1992. Antiatherogenic effects of L-arginine in the hypercholesterolemic rabbit. *J. Clin. Invest.* **90**:1168–1172.
3. Cooke, J.P., Andon, N.A., Girerd, X.J., Hirsch, A.T., and Creager, M.A. 1991. Arginine restores cholinergic relaxation of hypercholesterolemic rabbit thoracic aorta. *Circulation.* **83**:1057–1062.
4. Drexler, H., Zeiher, A.M., Meinzer, K., and Just, H. 1991. Correction of endothelial dysfunction in coronary microcirculation of hypercholesterolaemic patients by L-arginine. *Lancet.* **338**:1546–1550.
5. Candipan, R.C., Wang, B.Y., Buitrago, R., Tsao, P.S., and Cooke, J.P. 1996. Regression or progresssion. Dependency on vascular nitric oxide. *Arterioscler. Thromb. Vasc. Biol.* **16**:44–50.
6. Boger, R.H., et al. 1997. Dietary L-arginine reduces the progression of atherosclerosis in cholesterol-fed rabbits: comparison with lovastatin. *Circulation.* **96**:1282–1290.
7. Aji, W., et al. 1997. L-arginine prevents xanthoma development and inhibits atherosclerosis in LDL receptor knockout mice. *Circulation.* **95**:430–437.
8. Channon, K.M., et al. 1998. In vivo gene transfer of nitric oxide synthase enhances vasomotor function in carotid arteries from normal and cholesterol-fed rabbits. *Circulation.* **98**:1905–1911.
9. Qian, H., Neplioueva, V., Shetty, G.A., Channon, K.M., and George, S.E. 1999. Nitric oxide synthase gene therapy rapidly reduces adhesion molecule expression and inflammatory cell infiltration in carotid arteries of cholesterol-fed rabbits. *Circulation.* **99**:2979–2982.
10. Vasquez-vivar, J., et al. 1998. Superoxide generation by endothelial nitric oxide synthase: the influence of cofactors. *Proc. Natl. Acad. Sci. USA.* **95**:9220–9225.
11. Xia, Y., Tsai, A.L., Berka, V., and Zweier, J.L. 1998. Superoxide generation from endothelial nitric-oxide synthase. A Ca^{2+}/calmodulin-dependent and tetrahydrobiopterin regulatory process. *J. Biol. Chem.* **273**:25804–25808.
12. Ohashi, Y., et al. 1998. Hypotension and reduced nitric oxide-elicited vasorelaxation in transgenic mice overexpressing endothelial nitric oxide synthase. *J. Clin. Invest.* **102**:2061–2071.
13. Ozaki, M., et al. 2001. Reduced hypoxic pulmonary vascular remodeling by nitric oxide from the endothelium. *Hypertension.* **37**:322–327.
14. Kawashima, S., et al. 2001. Endothelial NO synthase overexpression inhibits lesion formation in mouse model of vascular remodeling. *Arterioscler. Thromb. Vasc. Biol.* **21**:201–207.
15. Breslow, J.L. 1996. Mouse models of atherosclerosis. *Science.* **272**:685–688.
16. Piedrahita, J.A., Zhang, S.H., Hagaman, J.R., Oliver, P.M., and Maeda, N. 1992. Generation of mice carrying a mutant apolipoprotein E gene inactivated by gene targeting in embryonic stem cells. *Proc. Natl. Acad. Sci. USA.* **89**:4471–4475.
17. Paigen, B., Morrow, A., Holmes, P.A., Mitchell, D., and Williams, R.A. 1987. Quantitative assessment of atherosclerotic lesions in mice. *Atherosclerosis.* **68**:231–240.
18. Shinozaki, K., et al. 2000. Oral administration of tetrahydrobiopterin prevents endothelial dysfunction and vascular oxidative stress in the aortas of insulin-resistant rats. *Circ. Res.* **87**:566–573.
19. Zhang, S.H., Reddick, R.L., Burkey, B., and Maeda, N. 1994. Diet-induced atherosclerosis in mice heterozygous and homozygous for apolipoprotein E gene disruption. *J. Clin. Invest.* **94**:937–945.
20. Kauser, K., da Cunha, V., Fitch, R., Mallari, C., and Rubanyi, G.M. 2000. Role of endogenous nitric oxide in progression of atherosclerosis in apolipoprotein E-deficient mice. *Am. J. Physiol. Heart. Circ. Physiol.* **278**:H1679–H1685.

21. Detmers, P.A., et al. 2000. Deficiency in inducible nitric oxide synthase results in reduced atherosclerosis in apolipoprotein E-deficient mice. *J. Immunol.* **165**:3430–3435.
22. Nagata, N., Momose, K., and Ishida, Y. 1999. Inhibitory effects of catecholamines and anti-oxidants on the fluorescence reaction of 4,5-diaminofluorescein, DAF-2, a novel indicator of nitric oxide. *J. Biochem. (Tokyo).* **125**:658–661.
23. Itoh, Y., et al. 2000. Determination and bioimaging method for nitric oxide in biological specimens by diaminofluorescein fluorometry. *Anal. Biochem.* **287**:203–209.
24. Qui, W., Kass, D.A., Hu, Q., and Ziegelstein, R.C. 2001. Determinants of shear stress-stimulated endothelial nitric oxide production assessed in real-time by 4,5-diaminofluorescein fluorescence. *Biochem. Biophys. Res. Commun.* **286**:328–335.
25. Yasui, H., and Sakurai, H. 2000. Chemiluminescent detection and imaging of reactive oxygen species in live mouse skin exposed to UVA. *Biochem. Biophys. Res. Commun.* **269**:131–136.
26. Skatchkov, M.P., Sperling, D., Hink, U., Anggard, E., and Munzel, T. 1998. Quantification of superoxide radical formation in intact vascular tissue using a Cypridina luciferin analog as an alternative to lucigenin. *Biochem. Biophys. Res. Commun.* **248**:382–386.
27. Hink, U., et al. 2001. Mechanisms underlying endothelial dysfunction in diabetes mellitus. *Circ. Res.* **88**:E14–E22.
28. Masada, M., Akino, M., Sueoka, T. and Katoh, S. 1985. Dyspropterin, an intermediate formed from dihydroneopterin triphosphate in the biosynthetic pathway of tetrahydrobiopterin. *Biochim. Biophys. Acta.* **840**:235–244.
29. Laursen, J.B., et al. 2001. Endothelial regulation of vasomotion in apoE-deficient mice: implications for interactions between peroxynitrite and tetrahydrobiopterin. *Circulation.* **103**:1282–1288.
30. Huang, A., Vita, J.A., Venema, R.C., and Keaney, J.F. 2000. Ascorbic acid enhances endothelial nitric-oxide synthase activity by increasing intracellular tetrahydrobiopterin. *J. Biol. Chem.* **275**:17339–17406.
31. Heller, R., et al. 2001. L-ascorbic acid potentiates endothelial nitric oxide synthesis via a chemical stabilization of tetrahydrobiopterin. *J. Biol. Chem.* **276**:40–47.
32. Wilcox, J.N., et al. 1997. Expression of multiple isoforms of nitric oxide synthase in normal and atherosclerotic vessels. *Arterioscler. Tromb. Vasc. Biol.* **17**:2479–2488.
33. Oemar, B.S., et al. 1998. Reduced endothelial nitric oxide synthase expression and production in human atherosclerosis. *Circulation.* **97**:2494–2498.
34. Knowles, J.W, et al. 2000. Enhanced atherosclerosis and kidney dysfunction in eNOS$^{-/-}$ApoE$^{-/-}$ mice are ameliorated by enalapril treatment. *J. Clin. Invest.* **105**:451–458.
35. Kuhlencordt, P.J., et al. 2001. Accelerated atherosclerosis, aortic aneurysm formation, and ischemic heart disease in apolipoprotein E/endothelial nitric oxide synthase double-knockout mice. *Circulation.* **104**:448–454.
36. Minor, R.L., Myers, P.R., Guerra, R., Bates, J.N., and Harrison, D.G. 1990. Diet-induced atherosclerosis increases the release of nitrogen oxides from rabbit aorta. *J. Clin. Invest.* **86**:2109–2116.
37. Kanazawa, K., et al. 1996. Endothelial constitutive nitric oxide synthase protein and mRNA increased in rabbit atherosclerotic aorta despite impaired endothelium-dependent vascular relaxation. *Am. J. Pathol.* **148**:1949–1956.
38. Dhalla, N.S., Temsah, R.M., and Netticadan, T. 2000. Role of oxidant stress in cardiovascular diseases. *J. Hypertens.* **18**:655–673.
39. Kojda, G., and Harrison, D.G. 1999. Interactions between NO and reactive oxygen species: pathophysiological importance in atherosclerosis, hypertension, diabetes, and heart failure. *Cardiovasc. Res.* **43**:562–571.
40. Cosentino, F., and Luscher, T.F. 1999. Tetrahydrobiopterin and endothelial nitric oxide synthase activity. *Cardiovasc. Res.* **43**:274–278.
41. Katusic, Z.S. 2001. Vascular endothelial dysfunction: does tetrahydrobiopterin play a role? *Am. J. Physiol. Heart. Circ. Physiol.* **281**:H981–H986.
42. Hong, H.J., Hsiao, G., Cheng, T.H., and Yen, M.H. 2001. Supplementation with tetrahydrobiopterin suppresses the development of hypertension in spontaneously hypertensive rats. *Hypertension.* **38**:1044–1048.
43. Kamada, Y., et al. 2001. Vascular endothelial dysfunction resulting from L-arginine deficiency in a patient with lysinuric protein intolerance. *J. Clin. Invest.* **108**:717–724. doi:10.1172/JCI200111260.
44. Niu, X.L., et al. 2001. Inducible nitric oxide synthase deficiency does not affect the susceptibility of mice to atherosclerosis but increases collagen content in lesions. *Circulation.* **103**:1115–1120.
45. Kuhlencordt, P.J., Chen, J., Han, F., Astern, J., and Huang, P.L. 2001. Genetic deficiency of inducible nitric oxide synthase reduces atherosclerosis and lowers plasma lipid peroxides in apolipoprotein E-knockout mice. *Circulation.* **103**:3099–3104.

Circ J 2004; **68:** 677–682

Identification of Autoantibodies With the Corresponding Antigen for Repetitive Coxsackievirus Infection-Induced Cardiomyopathy

Satoko Takata, MD; Hiroshi Nakamura, MD; Seiji Umemoto, MD; Kazuhito Yamaguchil, DVM*; Taichi Sekine, MSc**; Tomohiro Kato, MD**; Kusuki Nishioka, MD**; Masunori Matsuzaki, MD

Background The hypothesis that viral myocarditis causes an autoimmune response and subsequent dilated cardiomyopathy is controversial. To further investigate the autoimmune mechanism of cardiac dilatation and dysfunction after repeated episodes of viral myocarditis, the cardiac autoantigens induced by repetitive coxsackievirus B3 (CVB3) infection were examined.

Methods and Results Male inbred A/J mice were inoculated intraperitoneally with CVB3 at 3 and 40 weeks of age. At 8 weeks after the second inoculation, the mortality of the repetitive CVB3 group was significantly increased compared with that of the control group, and was associated with a significant reduction in fractional shortening and marked left ventricular dilatation without inflammatory cell infiltration. The cardiac antigens in the repetitive CVB3 infection were identified by 2-dimensional electrophoresis and subsequent liquid chromatography/tandem mass spectrometry (LC-MS/MS) using the serum at 2 weeks after the second inoculation. LC-MS/MS and immunohistochemistry demonstrated α-cardiac actin and heat shock protein 60 (HSP60) as cardiac near-surface antigens induced by the repetitive CVB3 infection. Immunoelectron microscopy disclosed the selective localization of anti-IgM antibody on the membrane of the myocytes in the repetitive CVB3 group.

Conclusions IgM antibodies against α-cardiac actin and HSP60, which were induced by repetitive CVB3 infection, may play an important role in the pathophysiology of the subsequent cardiac dysfunction and dilatation. (*Circ J* 2004; **68:** 677–682)

Key Words: Autoantigen; Autoimmunity; Coxsackievirus; HSP60; Viral Myocarditis

Dilated cardiomyopathy (DCM) is characterized by the dilatation and impaired contraction of the ventricles and clinically progressive heart failure[1] It may be idiopathic, familial/genetic, viral and/or immune, alcoholic/toxic, or associated with recognized cardiovascular disease in which the degree of myocardial dysfunction is not explained by the abnormal loading conditions or the extent of ischemic damage. Although the relationship between viral myocarditis and DCM remains controversial, a causal link has become more evident because of the tremendous developments in the molecular analyses of autopsy and endomyocardial biopsy specimens, new techniques of viral gene amplification, and advances in modern immunology[2,3]

It has already been reported that an autoimmune response plays a key role in the progression after viral myocarditis[3,4] This occurs in the context of a polyclonal stimulation of the immune system after the initial viral assault that may have been already cleared when the autoreactive B- and T-cell response occurs[5] Recently, we demonstrated that repetitive coxsackievirus B3 (CVB3) infection produced cardiac dilatation without inflammatory cell infiltration in the heart of mice with post-myocarditis, and autoimmunity mediated by the circulation of certain antibodies (eg, antibodies against the CVB3 genome or a CVB3-related protein) may be part of the pathogenic mechanism for this phenomenon. Moreover, only the autoreactive IgM antibody was apparent on the cell membrane of the myocytes and interstitial tissue in the repetitive infected mice, and may play a pivotal role in the early response to the virus in our repetitive viral myocarditic mice[6] To identify the autoantigen against the components of the myocardium in repetitive CVB3 myocarditic mice, particularly targeting the cell membrane, we examined whether IgM type-autoantibodies were present in the serum of these animals.

Methods

The experimental protocols used in this study were approved by the Ethics Committee for Animal Experimentation at Yamaguchi University School of Medicine, and carried out according to the Guidelines for Animal Experimentation at Yamaguchi University School of Medicine, and Law No. 105 and Notification No. 6 of the Japanese Government.

(Received November 28, 2003; revised manuscript received April 27, 2004; accepted April 30, 2004)

*Department of Cardiovascular Medicine and *Institute of Laboratory Animals, Yamaguchi University Graduate School of Medicine, Ube, and **Division of Rheumatology, Immunology and Genetics Program, Institute of Medical Science, St Marianna University School of Medicine, Kawasaki, Japan*

Mailing address: Masunori Matsuzaki, MD, PhD, Department of Cardiovascular Medicine, Yamaguchi University Graduate School of Medicine, 1-1-1 Minami Kogushi, Ube, Yamaguchi 755-8505, Japan. E-mail: ninai@yamaguchi-u.ac.jp

Experimental Protocol

Three-week old, inbred, certified, virus-free A/J (H-2a) male mice were purchased from Japan SLC (Shizuoka, Japan). Fourteen normal mice were also housed for 40 weeks as a control (3W–/40W–). The CVB3 (Nancy strain) was obtained from the American Type Culture Collection and stored at –80°C until use. Each 3-week old mouse was initially infected by an intraperitoneal injection of 2×10^4 plaque-forming units of CVB3 in 0.2 ml of saline. The infected mice were isolated, 5 per cage, in a special unit for 37 weeks (3W+/40W–). A total of 31 mice first inoculated at 3 weeks were reinfected in the same manner with CVB3 at 40 weeks (3W+/40W+). In addition, 5 normal mice were inoculated at 40 weeks (3W–/40W+) as a further control group. At 8 weeks after reinfection, the mice were weighed and killed with KCl injection via the inferior vena cava to stop the heart in end-diastole. Body weight was measured, and the hearts, lungs, and livers were excised and weighed. The control mice were treated in the same manner, but with saline that did not contain the virus.

Morphometry and Histopathological Study

The ventricles from the mice killed at 8 weeks after the second inoculation were halved transversely and one portion was fixed with 10% formalin solution, then embedded in paraffin solution and sectioned into slices of 4-mm thickness stained with hematoxylin-eosin and Azan solutions. The left ventricular (LV) dimensions and wall thickness were measured using the transverse section of the middle portion of the ventricle. The cavity dimensions and wall thickness of the left ventricle were calculated according to the method of Matsumori et al7 Cardiac fibrosis was also evaluated quantitatively using a Fotovision FV-10 camera (Fuji Film Co, Japan) and a (Macintosh 8500/120) computer equipped with NIH Image version 1.62 software.

Echocardiography

Prior to death at 8 weeks after the second inoculation, the mice underwent light anesthesia with ether. The LV end-diastolic dimension (EDD), end-systolic dimension (ESD), and fractional shortening (%FS) were obtained by averaging the data from 3 cardiac cycles using an echocardiographic system (ALOKA 5500; Aloka, Japan) with a dynamically focused 10-MHz linear array transducer.

Immunoelectron Microscopy

Immunoelectron microscopy was performed by the method of Yamaguchi et al[8] Briefly, the hearts at 2 weeks after the second inoculation were fixed by perfusing with paraformaldehyde. For immunostaining, horseradish peroxidase (HRP) conjugated anti-mouse IgM was used. Sections 10–19 nm thick were examined with a JEOL 200 CX transmission electron microscope at 160 kV. Sarcomere lengths were measured in a blinded fashion at a magnification of 3,700. This process was repeated for 50 fields per animal.

Two-Dimensional Western Blotting

Fresh murine heart tissue at 2 weeks after the second inoculation was minced and resuspended in 5 volumes of STE buffer containing 320 mmol/L sucrose, 10 mmol/L Tris–HCl, pH 7.4, 1 mmol/L EGTA, 5 mmol/L NaN3, 10 mmol/L -mercaptoethanol, 20 mmol/L leupeptin, 0.15 mmol/L pepstatin A, 0.2 mmol/L phenylmethylsulfonyl fluoride, and 50 mmol/L NaF, with a Polytron homogenizer (PT1200; Kinematica, Germany), at its maximum speed for 30 s, repeated 3 times. Homogenates were mixed with an equal volume of STE buffer and centrifuged at 1,000 G for 10 min, and the supernatant was centrifuged at 100,000 G for 60 min. The 1,000-G and 100,000-G pellets were designated as P1 and P2 fractions, respectively, and the 100,000-G supernatant as the S fraction. The P1 and P2 fractions were resuspended in STE buffer. The total protein concentration in each fraction was determined, using bovine serum albumin as a standard[9]

The extracted protein samples were diluted in a rehydration buffer (8 mol/L urea, 2% CHAPS, 2.8 mg/ml dithiothreitol (DTT), trace of bromphenol blue) containing 0.5% immobilized pH gradient (IPG) buffer (pH range 3–10; Amersham Pharmacia Biotech, Sweden), and loaded onto 7 cm Immobiline Drystrips (Amersham Pharmacia Biotech) in the IPG reswelling tray (Amersham Pharmacia Biotech) at room temperature overnight. Up to 400 mg of the extracted proteins was applied onto the drystrip gels for western blotting, and up to 1,000 mg for the analysis by mass spectrometry. Isoelectric focusing (IEF) was performed in a horizontal electrofocusing apparatus (MultiPhor II; Pharmacia Biotech, Sweden) according to the manufacturer's instructions. After the IEF, the IPG strips were equilibrated in 2 equilibration solutions. The first equilibration solution consisted of 10 mg DTT per 1 ml sodium dodecyl sulfate (SDS) equilibration buffer (1.5 mol/L Tris-Cl, pH8.8; 6 mol/L urea, 30% glycerol, 2% SDS), and the second equilibration solution consisted of 25 mg iodoacetamide per 1 ml SDS equilibration buffer. The equilibrated strips were placed on top of a 12.5% SDS polyacrylamide gel electrophoresis (PAGE) slab and sealed with 0.5% lower melt gel, and then the second electrophoresis was performed with a 40 mA constant current in the separating gel at 20°C.

After electrophoresis, the SDS-PAGE gels were stained with Coomassie Brilliant Blue (CBB) or used for protein transfer onto nitrocellulose membranes (Protran, Schleicher & Schuell, Germany). In the western blotting, the membranes were blocked in phosphate-buffered saline (PBS) containing 1% bovine serum albumin (BSA) and 0.1% Tween 20 for 1 h, washed in PBS with 0.1% Tween 20 (PBST) for 30 min, and incubated with serum samples, which were collected from mice at 2 weeks after the second inoculation, diluted adequately in PBST containing 1% BSA for 1 h. After 5 washings in PBST, the bound antibodies were reacted with HRP-conjugated goat anti-mouse IgM (Sigma, St Louis, MO, USA) for 1 h. Finally, the bound antibodies were visualized by diaminobenzidine.

Mass Determination and Mass Fingerprinting

Liquid chromatography/tandem mass spectrometry (LC-MS/MS) was performed as follows to determine the molecular weight of the protein spots. Protein spots on the gel stained with CBB, which corresponded to the positive spots on the western blotting membranes, were recovered and then the recovered gel fragments were washed in double distilled water for 15 min, de-colored in 50 ml decoloring solution (0.1 mol/L ammonium hydrogen carbonate, 50% methanol) at 40°C for 15 min, and cut into small pieces. The gel pieces were re-hydrated in 20 ml trypsin solution (0.1 pmol/ml trypsin in 50 mmol/L Tris-HCl; Wako Pure Chemical Industries, Ltd, Japan) and incubated at 37°C. The digested peptides were extracted from the gel pieces using trifluoroacetic acid (TFA) and acetonitrile.

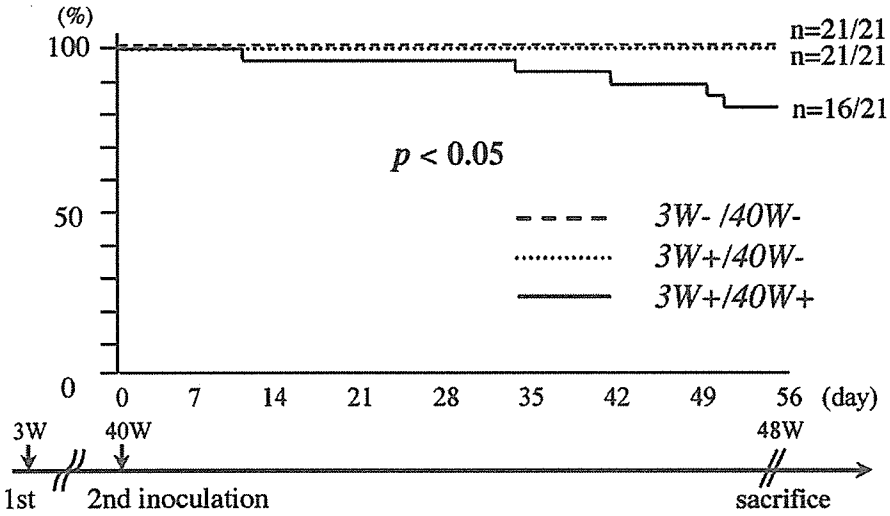

Fig 1. Survival curve after the second inoculation in viral myocarditic mice at 40 weeks. A survival reduction of 23.8% was observed in the repetitive group (3W+/40W+) compared with the control group (3W–/40W–) at 8 weeks after the second inoculation. *p<0.05 vs both the 3W–/40W– and 3W+/40W– groups. No mice died after the second vehicle injection.

Specifically, the digested products were added to 50 ml of 0.1% TFA/50% acetonitrile, vortexed, and sonicated for 10 min. After centrifugation, the supernatant was recovered. After 2 more cycles of this extraction, a similar extraction was performed with 50 ml of 0.1% TFA/80% acetonitrile. The collected supernatant was centrifuged again, filtered, and concentrated down to 50 ml in an evaporator, and was then desalted using a Zip-Tip desalting column (Millipore Corp, Milford, MA, USA). The peptide sample solution was stored at –20°C until mass spectrometry analysis.

The mass of the digested peptides in the samples was determined using a mass spectrometer with matrix-assisted laser desorption/ionization-time of flight (MALDI-TOF: Voyager DE-STR; PerSeptive Biosystems, USA). Alpha-cyano-4-hydroxycinnamic acid was used as an assisting matrix. A list of the determined peptide masses was made by a mass fingerprint search of the NCBI protein databases using the Mascot software program (Matrix Science, Ltd, UK), in which the NCBI protein databases were searched.

Immunohistochemistry

For immunoenzymatic staining, the remaining ventricular portion was quickly frozen with OCT compound (Miles, Inc, USA) in liquid nitrogen and stored at –80°C. The frozen specimens were sectioned at 4-mm thickness. Immunoenzymatic staining was performed with a DAKO LSAB kit (DAKO, USA) according to the manufacturer's instructions. Antibody against murine heart shock protein 60 (HSP60) (Stressgen, Canada) was used as the primary antibody.

Statistical Analysis

Data were expressed as the mean±SD. Statistical analysis of the data was performed by an analysis of variance with multiple comparisons. The survival of all animals was assessed by Kaplan-Meier analysis. A level of $p<0.05$ was considered statistically significant.

Results

Survival Rates

Fig 1 shows the survival curve at 8 weeks after the second inoculation at 40 weeks. Five of the 21 mice died after the second CVB3 inoculation (mortality rate: 23.8%, $p<0.05$). All of the dead mice had pleural effusion and ascites, indicating that they probably died from heart failure. No mice died after the second vehicle injection.

Table 1 Assessment of the Systemic Parameters of Viral Myocarditis

	Group		
	3W–/40W–	3W+/40W–	3W+/40W+
Physiological analysis			
No. of experiments	5	5	5
Body weight (g)	29.2±2.8	30.2±2.5	26.3±2.0†
Heart weight (mg)	108±4.2	140.8±38.4	201.4±91.0*
Lung weight (mg)	212±3.6	199±92	221±93
Liver weight (mg)	1,173±268	1,023±101	967±4
HW/BW(mg/g)	3.73±0.45	4.65±1.11	7.89±4.15*
LW/BW (mg/g)	7.25±0.90	6.55±2.75	8.5±4.38
LIW/BW (mg/g)	40.21±8.31	34.21±2.44	36.28±1.99
Morphometry			
Wall thickness (mm)	0.8±0.1	0.7±0.1	0.7±0.1
Fibrosis (%)	3.1±0.7	16.5±11.1*	26.9±6.0*†
Inflammatory grading	0	0.2±0.4	0.2±0.4
Echocardiography			
LVEDD (mm)	2.4±0.3	2.6±0.4	3.4±0.3*†
LVESD (mm)	0.9±0.1	1.3±0.3*	2.4±0.5*†
%FS (%)	60.8±5.4	50.6±7.6*	29.6±7.9*

HW/BW, ratio of heart weight/body weight; LW/BW, ratio of lung weight/body weight; LIW/BW, ratio of liver weight/body weight; LVEDD, left ventricular end-diastolic dimension; LVESD, left ventricular end-systolic dimension; %FS, fractional shortening.
*Values are the mean±SD. *p<0.05 vs the 3W–/40W– group. †p<0.05 vs the 3W+/40W– group.*

Physiological Analysis

The mean body weight in the 3W+/40W+ group was significantly reduced compared with that in the 3W+/40W– group ($p<0.05$). The heart weight and the ratio of heart weight/body weight in the 3W+/40W+ group was significantly increased compared with that in the 3W–/40W– group ($p<0.05$) (Table 1). There were no differences between the 3W–/40W– and 3W+/40W– groups in body weight or heart weight, or in the ratio of the heart weight/body weight. In addition, there were no significant differences in the weights of the lungs and livers among the 3 groups.

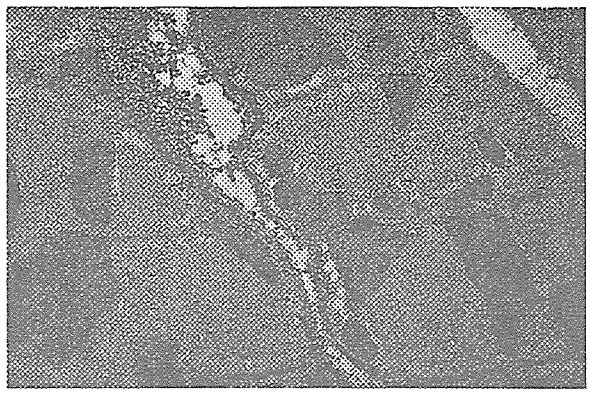

Fig 2. Ultrastructural localization of anti-heart antibodies was confirmed on the surface of the myocytes and interstitial tissue with immunoelectron microscopy (×10,000).

Histology

There was a significant increase in the LV dimension in the 3W+/40W+ group compared with the 3W+/40W– group ($p<0.05$). The ratio of cardiac fibrosis in the 3W+/40W– and 3W+/40W+ groups was significantly higher than in the 3W–/40W– group ($p<0.05$). The ratio of cardiac fibrosis in the 3W+/40W+ group was the highest among the 3 groups (Table 1). There was no significant difference in the mean wall thickness among the 3 groups. Inflammatory cell infiltration was less than 5% in all groups (Table 1).

Echocardiography

To evaluate cardiac function, we performed transthoracic echocardiography at 8 weeks after the second inoculation. Both the LVEDD and LVESD of the 3W+/40W+ group were significantly increased compared with those of the other 2 groups; %FS was significantly reduced in the 3W+/40W+ group compared with that in the other 2 groups (Table 1).

Immunoelectron Microscopy

The sarcomere length in the 3W+/40W+ group was 1.8±0.24 mm, which is comparable to the data previously obtained[6] Staining of bound IgM in the myocardium was recognized only in the 3W+/40W+ group. The cell membranes of the myocytes and interstitial tissue were positively stained with the anti-IgM antibody by immunoelectron microscopy (Fig 2).

Two-Dimensional Western Blotting and Subsequent LC-MS/MS

On 2-dimensional western blotting, 2 spots were detected as A3 (pI 5.2) and A5 (pI 5.9) in the membranous fraction that specifically cross-reacted with the serum in the 3W+/40W+ group (Fig 3). By subsequent LC-MS/MS, A3 (MW 42001 Da) and A5 (MW 60941 Da) were recognized as a-cardiac actin and HSP60, respectively (Fig 3).

Immunohistochemistry

Because α-cardiac actin is known to be ubiquitously distributed in myocytes, and only HSP60 is reported to be upregulated on the cell surface, as well as in the cytosol and mitochondria in response to many different stresses,[10] we performed further immunohistochemical analysis for HSP60 at 2 weeks after the second inoculation. We showed that HSP60 was positively stained in the myocytes and interstitial tissue (yielding a brown color with a pale blue background) taken from the hearts in the 3W+/40W+ group (Fig 4A). No myocytes were positively stained with the HSP60 antibody in the 3W–/40W–, 3W+/40W– or 3W–/40W+ groups (Fig 4B,C and 4, respectively).

Discussion

There is some clinical evidence that DCM is a late sequel of acute or chronic viral myocarditis[5] Infectious and autoimmune myocarditis has also been extensively proven using murine and rat models[3–5] We previously demonstrated that repetitive CVB3 infection in mice could cause LV dilatation with dysfunction through autoantibodies,

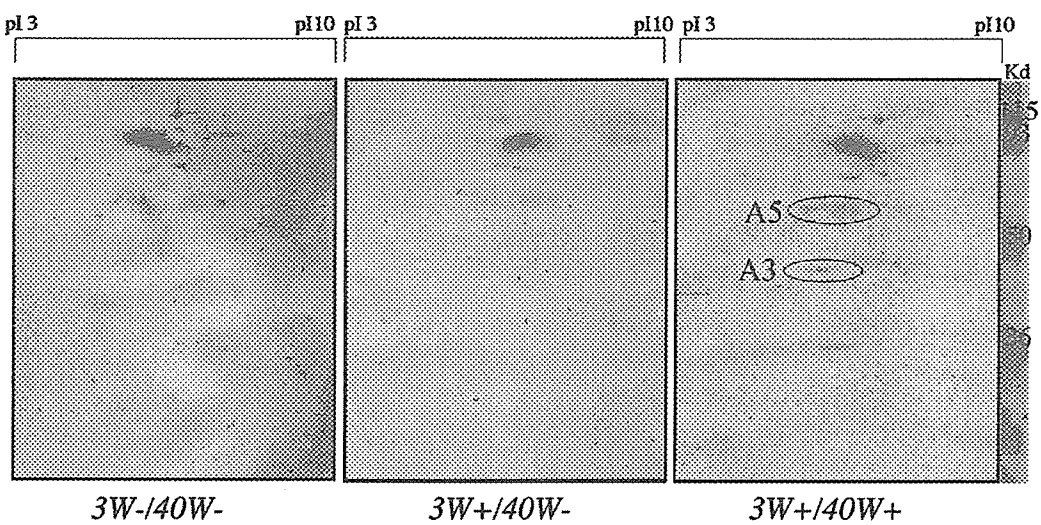

Fig 3. Two-dimensional western blotting with the serum in the 3W–/40W–, 3W+/40W–, and 3W+/40W+ groups. Two spots were detected as A3 and A5 in the membranous fraction that specifically cross-reacted with the serum in the 3W+/40W+ group compared with the other 2 groups. A3 and A5 were recognized as α-cardiac actin and murine HSP60, respectively, by subsequent LC-MS/MS.

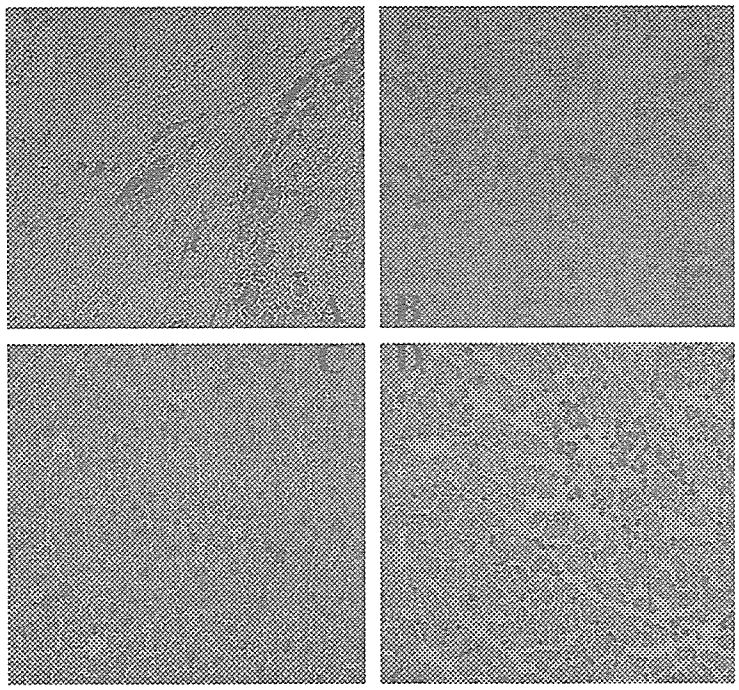

Fig 4. Immunohistochemistry of the myocardium with the anti-HSP60 antibody. The HSP60-positive cells were scattered in the myocardium in the 3W+/40W+ mouse (A). No specific staining for the anti-HSP60 antibody was observed in the heart tissue of either the 3W–/40W– (B), 3W+/40W– (C), or 3W–/40W+ (D) groups.

which were immunologically maximally activated at 2 weeks after the second CVB3 inoculation[6] Moreover, these pathophysiological changes were present even at 8 weeks after the second inoculation. Electron microscopy showed that these antibodies belong to the IgM subtype, and were distributed on the surface of the myocytes and interstitial tissue at 2 weeks after the second viral inoculation in mice. The results of our study are entirely different from the previously reported anti-heart antibodies in viral myocarditis[5] First, in the present study repetitive CVB3 infection produced cardiac dilatation and dysfunction without inflammatory cell infiltration in post-myocarditic mice. This poor T cell response may be related to the protective effect of neutralizing antibody against CVB3 induced by the first inoculation, as well as to CVB3 being less able to cause myocardial lesions related to senescence[6] Second, antibodies that react to the membranous fraction of normal myocytes were produced in the repetitive viral infection, but not in the post-myocarditis mice with simple viral infection. Third, the antibodies were classified as the IgM subtype, as distinct from the other IgG-type antibodies, such as ADP-ATP carrier protein and cardiac sarcoplasmic reticulum calcium ATPase, which were previously identified as cardiac autoantibodies[5] Fourth, the antibodies reacted to the membrane fraction of the myocytes, so that these antibodies identified in the serum of the repetitive myocarditic mice could easily bind the targeting antigen and cause immunological cytotoxicity accompanied by activation of the complementary system in vivo![11] It has also been reported that some anti-heart IgM autoantibodies can activate the complementary system and cause subsequent cardiac damage, especially in membranous proteins such as myolemmal![12] Fifth, we identified 2 autoantibodies (α-cardiac actin and HSP60) against the cardiac membrane protein. Finally, we have already reported that interleukin-1α and tumor necrosis factor-α were elevated in our model[6] They are able to potentiate the immune response and induce cell death, both of which appear to have a special importance in the pathogenesis of myocarditis. As a result, the IgM antibodies, which can activate the complementary system, and cytokines may cooperatively cause the cytotoxic effect on the target myocytes.

In patients with histologically proven myocarditis or familial DCM, autoreactive autoantibodies to components of the myocardium are often present, including intracellular targets such as the ADP/ATP translocator and other mitochondrial proteins![13] Dorffel et al demonstrated that the extraction of autoimmunoreactive antibodies by immunoadsorption results in a functional improvement in hemodynamics in DCM patients![14] Those authors have proven indirectly that autoantibodies against the ADP-ATP carrier![15] contractile proteins of cardiomyocytes, and the cardiac β_1-adrenergic receptor[16,17] contribute to cardiac malfunction in DCM. They proposed that the immunoadsorption may be an additional therapeutic possibility for the acute hemodynamic stabilization of patients with severe DCM. Moreover, Kishimoto et al reported that antibody-mediated immune enhancement is involved in the pathogenesis of CBV3 myocarditis in mice![18] Nishimura et al also proved that PD-1, which binds to the 33-kD protein, may be an important factor contributing to autoimmune cardiomyopathy in mice![19] These results raise the possibility that some form of cardiomyopathy may have a CVB3-induced autoimmune basis, and that identifying possible autoantigen(s) may open up new diagnostic and therapeutic approaches for this disease. Regarding their results, molecular mimicry may be involved in these mechanisms?[20] This occurs when an immune response mounted by the host against a specific determinant of an infecting viral or bacterial agent cross-reacts with a similar 'mimicked' host sequence, leading to autoimmunity, and, in some cases, tissue injury and disease. However, one question that has been raised is how these antibodies recognize cytosolic antigen in intact myocytes, because these antigens are isolated and tolerated from circulating antibodies![11] Interestingly, Maish et al demonstrated that anti-membrane antibodies circulated not only in

the peripheral blood, but were also bound to the sarcolemma and interstitial tissue in the endomyocardial biopsy specimens of patients[5] Their results are compatible with our electron microscopy findings, indicating that the antibodies belong to the IgM subtype, and respond to the surface of the myocytes in repetitive CVB3 infection. In this study, we compared the serum of repetitive CVB3 with other groups to identify autoantigens in the myocardium, and identified 2 cardiac antigens in the membranous fraction: α-cardiac actin and HSP60. Although α-cardiac actin is a well-known cytosolic component of myocytes, there is a technical limitation to purifying the membrane fraction in the process of extraction from a heart sample[9] As we observed in our study, α-cardiac actin has already been reported as a cytosolic autoantigen in CVB3 myocarditis[21]

In this study, we demonstrated that HSP60 may be a candidate for a membrane-bound autoantigen in repetitive CVB3 inoculation. The HSP family has been identified as a prominent target of ongoing immune responses during microbial infections. Cross-reactive immune responses between mammalian and microbial HSPs have been suggested as underlying several autoimmune and inflammatory disorders, including chronic arthritis, systemic lupus erythematosus, atherosclerosis, Crohn's disease, and diabetes[22] In addition to constituting an endogenous stress response that protects cells from injury, members of the HSP family are also candidate molecules that potentially signal tissue damage or cellular stress to the immune system, the so-called 'danger theory'. The expression of HSP is upregulated rapidly during several forms of cellular stress, and HSP can be released from damaged tissue[23] Portig et al reported that antibodies against HSP60 were found in the sera of patients with DCM, and may interfere with the functions this stress protein plays in cell physiology (ie, protein transport, protein maturation, and protection of the cell under stress conditions)[24] Latif et al also reported that not only was the anti-heart antibody against HSP60 present in the sera, but HSP60 was upregulated in the myocardium of patients with DCM[10] They confirmed that the cell surface expression of HSP60 after heat stress can be visualized using immunofluorescence. Taken together with our results, these findings suggest that IgM antibodies against α-cardiac actin and HSP60, which were induced by repetitive CVB3 infection, may play an important role in the pathophysiology of the subsequent cardiac dysfunction and dilatation.

Conclusions

In the present study, repetitive CVB3 infection caused cardiac dysfunction and dilatation with an induction of a variety of anti-heart antibodies. Exploring the nature of these autoantibodies found in the sera of our model will provide further immunological and virological insights into the mechanism of subsequent DCM after viral myocarditis.

Acknowledgments

We would like to thank Dr Akira Matsumori (Kyoto University, Kyoto, Japan) for his provision of CVB3. In addition, we would like to thank Rie Ishihara and Kazuko Iwamoto for their excellent technical assistance. This study was supported in part by funds from the Idiopathic Cardiomyopathy Research Group of the Ministry of Health and Welfare of Japan.

References

1. Kriett JM, Kaye MP. The registry of the international society for heart transplantation: Seventh official report, 1990. *J Heart Transplant* 1990; **9:** 323–330.
2. Kawai C. From myocarditis to cardiomyopathy: Mechanisms of inflammation and cell death: Learning from the past for the future. *Circulation* 1999; **99:** 1091–1100.
3. Nakamura H, Yamamura T, Umemoto S, Fukuta S, Shioi T, Matsumori A, et al. Autoimmune response in chronic ongoing myocarditis demonstrated by heterotopic cardiac transplantation in mice. *Circulation* 1996; **94:** 3348–3354.
4. Nakamura H, Kato T, Yamamura T, Yamamoto T, Umemoto S, Sekine T, et al. Characterization of T cell receptor b chains of accumulating T cells in chronic ongoing myocarditis demonstrated by heterotopic cardiac transplantation in mice. *Jpn Circ J* 2001; **65:** 106–110.
5. Maisch B, Ristic AD. Humoral immune response in viral myocarditis. *In*: Cooper LT, editor. Myocarditis: From bench to bedside. New Jersey: Humana Press; 2002; 77–108.
6. Nakamura H, Yamamoto T, Yamamura T, Nakao F, Umemoto S, Shintaku T, et al. Repetitive coxsackievirus infection induces cardiac dilatation in post-myocarditic mice. *Jpn Circ J* 1999; **63:** 794–802.
7. Matsumori A, Kawai C. An experimental model for congestive heart failure after encephalomyocarditis virus myocarditis in mice. *Circulation* 1982; **65:** 1230–1235.
8. Yamaguchi K, Takahashi S, Sasaki K, Tonosaki A. Early expression of intercellular adhesion molecule-1 in the corneal endothelium stimulated by endotoxin: An immuno-scanning electron microscopical study. *Jpn J Ophthalmol* 1996; **40:** 12–17.
9. Kawamura S, Yoshida K, Miura T, Mizukami Y, Matsuzaki M. Ischemic preconditioning translocates PKC-δ and -ε, which mediate functional protection in isolated rat heart. *Am J Physiol* 1998; **275:** 2266–2271.
10. Latif N, Taylor PM, Khan MA, Yacoub MH, Dunn MJ. The expression of heat shock protein 60 in patients with dilated cardiomyopathy. *Basic Res Cardiol* 1999; **94:** 112–119.
11. Wraith DC. Immunological tolerance. *In*: Roitt I, Brostoff J, Male D, editors. Immunology, 5th edn. London: Mosby; 1996; 187–198.
12. Olson TM, Kishimoto Y, Whitby FG, Michels VV. Mutations that alter the surface charge of alpha-tropomyosin are associated with dilated cardiomyopathy. *J Mol Cell Cardiol* 2001; **33:** 723–732.
13. Liu PP, Mason JW. Advances in the understanding of myocarditis. *Circulation* 2001; **104:** 1076–1082.
14. Dorffel WV, Felix SB, Wallukat G, Brehme S, Bestrvater K, Hofmann T, et al. Short-term hemodynamic effects of immunoadsorption in dilated cardiomyopathy. *Circulation* 1997; **95:** 1994–1997.
15. Schulze K, Becker BF, Schauer R, Schultheiss HP. Antibodies to ADP-ATP carrier, an autoantigen in myocarditis and dilated cardiomyopathy, impair cardiac function. *Circulation* 1990; **81:** 959–969.
16. Magnusson Y, Marullo S, Hoyer S, Waagstein F, Andersson B, Vahlne A, et al. Mapping of a functional autoimmune epitope on the β1-adrenergic receptor in patients with idiopathic dilated cardiomyopathy. *J Clin Invest* 1990; **86:** 1658–1663.
17. Baba A, Yoshikawa T, Chino M. Characterization of anti-myocardial autoantibodies in Japanese patients with dilated cardiomyopathy. *Jpn Circ J* 2001; **65:** 867–873.
18. Kishimoto C, Kurokawa M, Ochiai H. Antibody-mediated immune enhancement in coxsackievirus B3 myocarditis. *J Mol Cell Cardiol* 2002; **34:** 1227–1238.
19. Okazaki T, Tanaka Y, Nishio R, Mitsuiye T, Mizoguchi A, Wang J, et al. Autoantibodies against cardiac troponin I are responsible for dilated cardiomyopathy in PD-1-deficient mice. *Nat Med* 2003; **9:** 1477–1483.
20. Richardson P, McKenna W, Bristow M, Maisch B, Mautner B, O'Connell J, et al. Report of the 1995 World Health Organization/International Society and Federation of Cardiology Task Force on the definition and classification of cardiomyopathies. *Circulation* 1996; **93:** 841–842.
21. Maisch B, Bauer E, Cirsi M, Kochsiek K. Cytolytic cross-reactive antibodies directed against the cardiac membrane and viral proteins in coxsackievirus B3 and B4 myocarditis: Characterization and pathogenetic relevance. *Circulation* 1993; **87**(Suppl 4)**:** IV-49–IV-65.
22. Oldstone MB. Molecular mimicry and autoimmune disease. *Cell* 1987; **50:** 819–820.
23. Wallin RP, Lundqvvist A, More SH, von Bonin A, Kiessling R, Ljunggren HG. Heat-shock proteins as activators of the innate immune system. *Trends Immunol* 2002; **23:** 130–135.
24. Portig I, Pankuweit S, Maish B. Antibodies against stress protein in sera of patients with dilated cardiomyopathy. *J Mol Cell Cardiol* 1997; **29:** 2245–2251.

Original Article

Comparison of Gene Expression Profiling in Pressure and Volume Overload–Induced Myocardial Hypertrophies in Rats

Hiroshi MIYAZAKI[1], Naoki OKA[1], Akimasa KOGA[1], Haruya OHMURA[1], Tamenobu UEDA[1], and Tsutomu IMAIZUMI[1),2)]

Gene expression profiling has been conducted in rat hearts subjected to pressure overload (PO). However, pressure and volume overload produce morphologically and functionally distinct forms of cardiac hypertrophy. Surprisingly, gene expression profiling has not been reported for in an animal model of volume overload (VO). We therefore compared the gene expression profiles in the hypertrophied myocardium of rats subjected to PO and VO using DNA chip technology (Affymetrix U34A). Constriction of the abdominal aorta and abdominal aortocaval shunting were used to induce PO and VO, respectively. The gene expression profiles of the left ventricle (LV) 4 weeks after the procedure were analyzed by DNA chips. There were comparable increases in the left ventricular weight/body weight ratio in rats subjected to PO and VO. Echocardiography revealed concentric hypertrophy in the PO animals, but eccentric hypertrophy in the rats subjected to VO. The expressions of many genes were altered in VO, PO, or both. Among the genes that were upregulated in both forms of hypertrophy, greatly increased expressions of B-type natriuretic peptide, lysyl oxidase–like protein 1 and metallothionein-1 (MT) were confirmed by real-time reverse transcription–polymerase chain reaction (RT-PCR). Because free radicals are increased in the hypertrophied heart and may contribute to apoptosis, we examined the role of MT, a free radical scavenger, in apoptosis. The overexpression of MT in H9c2 cells inhibited norepinephrine-induced apoptosis, suggesting that MT may act as an anti-apoptotic molecule in cardiac hypertrophy. In conclusion, we found that many genes were regulated in VO, PO, or both. In addition, a novel role of MT in the hypertrophied myocardium was suggested. (*Hypertens Res* 2006; 29: 1029–1045)

***Key Words*: gene expression, hypertrophy, DNA chip, metallothionein-1, apoptosis**

Introduction

Pressure and volume overload (PO and VO, respectively) produce morphologically and functionally distinct forms of cardiac hypertrophy (*1–4*); PO produces concentric hypertrophy whereas VO produces eccentric hypertrophy. At the cellular level, cardiomyocytes grow vertically in PO and longitudinally in VO. The molecular mechanisms of these differences have been unknown. Changes of some specific genes have been reported in the hearts of PO and VO, *i.e.*, the expressions of collagen isoforms (*5*, *6*) and matrix metallo-

From the [1)]Department of Medicine, Division of Cardio-Vascular Medicine and [2)]Cardiovascular Research Institute, Kurume University School of Medicine, Kurume, Japan.

This study was supported in part by a grant from the Kimura Memorial Heart Foundation/Pfizer Grant for Research on Autonomic Nervous System and Hypertension (to N.O.), and a grant for Science Frontier Research Promotion Centers and a Grant-in-Aid for the Encouragement of Young Scientists (to H.M. and N.O.) from the Ministry of Education, Culture, Sports, Science and Technology, Japan.

Address for Reprints: Naoki Oka, M.D., Ph.D., Department of Medicine, Division of Cardio-Vascular Medicine, Kurume University School of Medicine, 67 Asahi-machi, Kurume 830–0011, Japan. E-mail: noka@med.kurume-u.ac.jp

Received February 27, 2006; Accepted in revised form September 4, 2006.

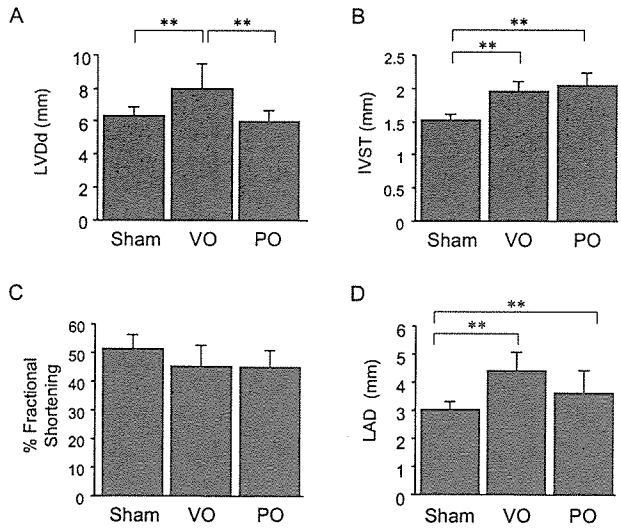

Fig. 1. *Echocardiographic measurements of the hypertrophied rat heart. Echocardiography was performed 28 days after hemodynamic overload as described in Methods. VO, volume overload group; PO, pressure overload group; LVDd, end-diastolic diameter of the left ventricle; IVST, interventricular septal wall thickness; %FS, percent fractional shortening; LAD, left atrial diameter. Values are the mean ±SD.* **p < *0.01* vs. *the sham group.*

proteinases (*7*), the expression of β myosin heavy chain (*8*), the transcriptional regulation of adrenomedullin (*9*), and the expressions of growth factors (*10*, *11*) and β-tubulin (*12*). Based on these previous reports, it is anticipated that some specific genes are regulated similarly or differentially in PO and VO, but the regulation of genes other than those listed above has not been clarified. Microarray analysis is a useful method to analyze the behavior of many genes. With this method, gene profiling has been conducted in animal hearts subjected to PO (*13*, *14*). Surprisingly, however, gene expression profiling has not been conducted in hearts subjected to VO. Accordingly, we compared the gene expression profiles in the hypertrophied myocardium of rats subjected to PO and VO using the DNA chip technology.

Methods

Animal Models

Male Wistar rats were used for the experiments. PO was produced in rats by abdominal aortic banding (*15*), and VO by aortocaval shunting (*16*). The rats were sacrificed 28 days after the procedure. All animal procedures were conducted according to the guidelines provided by the Kurume University Institutional Animal Care and Use Committee under an approved protocol.

Echocardiography

At the day before sacrifice, rats were lightly anesthetized with pentobarbital, then examined by echocardiography with an SSD 5500 and a 7.5 MHz probe (Aloka, Tokyo, Japan).

DNA Chip Analysis

DNA chips (GeneChip Rat Genome U34A arrays) were purchased from Affymetrix (Santa Clara, USA). Poly (A) RNA was extracted from the left ventricle (LV) by using a FAST track RNA purification kit (Invitrogen, Carlsbad, USA). We mixed poly (A) RNAs prepared from the LV of five rats and the samples were analyzed by three DNA chips in each group. DNA chip analysis was performed according to the manufacturer's recommended protocol. Each of the groups was compared with each of the other groups, resulting in 27 comparison tests. Average intensity values for each probe set were obtained from the Affymetrix MicroArray Suite 4.0. A p value less than 0.01 was arbitrarily assigned as the level of statistical significance. We considered genes that were elevated by >2 fold compared with controls as "upregulated," genes that were reduced to <0.5 as "downregulated," and genes that were altered by 0.8–1.2 fold as showing "no change." The genes that were expressed at very low levels (those with a signal intensity less than 100) or genes that were considered not to be present based on low signal intensity by the Affymetrix software under all conditions were omitted.

For clustering analysis, the CEL files were converted into DCP files using dCHIP analysis software (www.biostat.harvard.edu/compalab/cdhip/), as described previously by Li and Wong (*17*). Genechips were normalized, and model-based expression values were generated. We used hierarchical clus-

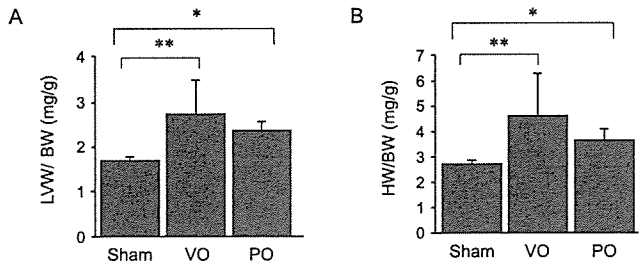

Fig. 2. *Left ventricular weight and heart weight 28 days after hemodynamic overload. A: LVW/BW. B: HW/BW. VO, volume overload group; PO, pressure overload group; LVW/BW, left ventricular weight normalized to body weight; HW/BW, heart weight normalized to body weight. Values are the mean±SD,* *p < *0.05,* **p < *0.01* vs. *the sham group.*

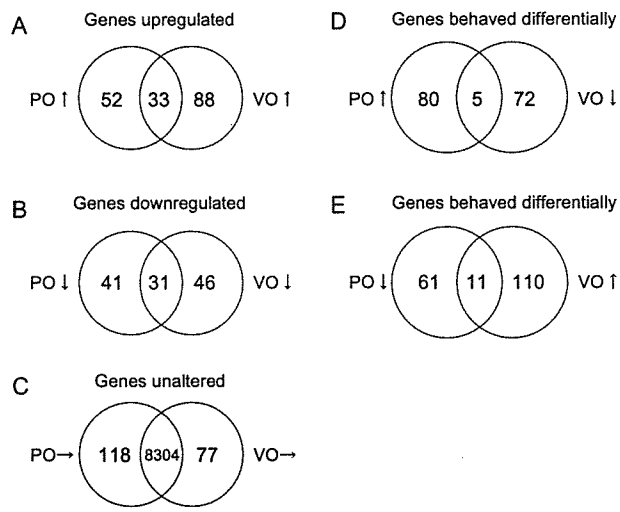

Fig. 3. *Comparisons of differentially regulated genes. Venn diagrams were produced to compare the number of genes altered in the volume overload (VO), pressure overload (PO), and sham groups. A: Genes differentially upregulated between the sham group and the VO group, PO group, or both. B: Genes differentially downregulated between the sham group and the VO group, PO group, or both. C: Genes unaltered between the sham group and the VO group, PO group, or both. D: Genes upregulated in the PO group, downregulated in the VO group, or both. E: Genes upregulated in the VO group, downregulated in the PO group, or both.*

tering with the average linkage method. The functions of these altered genes were classified by clusters of orthologous groups analysis.

Real-Time Reverse Transcription–Polymerase Chain Reaction

Total RNA was prepared with an RNeasy Midi Kit (QIAGEN, Tokyo, Japan) from LV. Real-time reverse transcription–polymerase chain reaction (RT-PCR) was performed by a GeneAmp 5700 and a TaqMan One-Step RT-PCR Master Mix Reagents Kit (Applied Biosystems, Foster City, USA) according to the manufacturer's instruction. Expression values for each gene were normalized to 18 S ribosomal RNA (TaqMan ribosomal RNA control reagents; Applied Biosystems). The primers and TaqMan probes used in these experiments were as follows: guanosine monophosphate (GMP) reductase TaqMan probe, CTCTGACGG AAGCTGCACATGTCCA; GMP reductase sense-primer, GGCCTCAAGGGACACATCA; GMP reductase antisense-primer, AAAGGCTTTGGCGACATCTC; metallothionein-1 (MT) TaqMan probe, TGCAAAGGTGCCTCGGACAAG TGC; MT sense-primer, GTGGGCTGCTCCAAATGTG; MT antisense-primer, GGTCCGGAAATTATTTACACC TGA; B-type natriuretic peptide (BNP) TaqMan Probe, CGGCGCAGTCAGTCGCTTGG; BNP sense-primer, TGG GCAGAAGATAGACCGGA; BNP antisense-primer, ACA ACCTCAGCCCGTCACAG; lysyl oxidase–like protein 1

Table 1. Genes That Respond to Pressure or Volume Overload

Accession	Probe set ID	Gene name	VO	PO	Molecular function	Reference
VO↑ and PO↑						
AA799773	rc_AA799773_at	Filamin C, γ	2.42	2.03	actin binding	*19*
AA892378	rc_AA892378_at	Similar to tetratricopeptide repeat domain 11 (LOC288584)	2.27	2.05	apoptosis	
S69383	S69383_at	12-Lipoxygenase	2.61	2.02	arachidonate 12-lipoxygenase activity, iron ion binding	*20*
L18948	L18948_at	S100 calcium-binding protein A9 (calgranulin B)	3.25	3.22	calcium ion binding	*19*
U17919	U17919_s_at	Allograft inflammatory factor-1	2.05	2.00	calcium ion binding	
AI102562	rc_AI102562_at	Metallothionein-1 (MT-1)	4.05	3.82	copper ion binding, metal ion binding, zinc ion binding	*14, 19, 21*
L16532	L16532_at	2′,3′-cyclic nucleotide 3′-phosphodiesterase (CnpII)	3.28	2.94	cyclic nucleotide catabolism	
U17254	U17254_g_at	Immediate early gene transcription factor NGFI-B	2.14	2.06	DNA binding, ligand-dependent nuclear receptor activity	
U75397	U75397UTR#1_s_at	Early growth response 1 (Egr 1)	2.37	2.03	DNA binding, nucleic acid binding, transcription factor activity	*21*
L22761	L22761_at	GATA binding protein 4 (Gata4)	2.42	3.06	DNA binding, transcription factor activity	*13*
AA859805	rc_AA859805_at	Lysyl oxidase like protein (LOXL)	3.95	2.48	elastogenesis	*19*
AA800517	rc_AA800517_s_at	Vesicle associated protein (VAP1)	2.07	2.02	endosome protein	
AI231472	rc_AI231472_s_at	Collagen α1 type I	3.67	3.90	extracellular matrix protein	*13, 14*
M17526	M17526_at	GTP (guanine nucleotide protein)-binding protein ($G_{\alpha}o$)	2.09	2.49	GDP binding	*19*
AA800784	rc_AA800784_at	Cysteine-rich protein 61 (CYR61)	2.18	2.18	growth factor binding, heparin binding	*14*
AA799498	rc_AA799498_at	Natriuretic peptide precursor type B	4.45	2.62	hormone activity	*13, 19, 22*
E00775	E00775cds_s_at	Natriuretic peptide precursor type A	4.12	2.56	hormone activity	*13, 14, 19, 20, 22*
M32062	M32062_at	Fc-γ receptor (IgG)	2.88	2.31	IgG binding, IgG receptor activity, receptor activity	
AI231213	rc_AI231213_at	Metastasis suppressor homolog (KAI1)	2.03	2.01	integral to membrane	
X04979	X04979_at	Apolipoprotein E	2.16	2.00	lipid transporter activity, lipid binding, heparin binding	
J00692	J00692_at	Skeletal muscle α-actin gene	2.47	2.02	motor activity, structural constituent of cytoskeleton	*14*
AA799678	rc_AA799678_s_at	EGL nine homolog 3	2.33	2.00	oxidoreductase activity	*19*
X71127	X71127_at	Complement protein C1q β-chain	2.23	2.00	phosphate transport, immune response, complement activation	
AI069982	rc_AI069982_s_at	Myotonic dystrophy kinase–related Cdc42-binding kinase (MRCK)	2.09	2.02	protein serine/threonine kinase activity	
AA875405	rc_AA875405_at	Forkhead-like 18	2.21	2.07	transcription, regulation of transcription, development	
AI639185	rc_AI639185_s_at	Potassium channel, subfamily K, member 3	3.20	3.26	transport, ion transport, potassium ion transport	
M91235	M91235_f_at	VL30 element	2.60	2.15	—	
AA892847	rc_AA892847_at	Similar to α-*N*-acetyl-galactosaminidase (LOC315165)	2.95	2.71	—	
AA891828	rc_AA891828_g_at	Similar to UV excision repair protein RAD23 homolog A	2.03	2.07	—	
AA799992	rc_AA799992_at	Similar to C11orf17 protein (LOC361624)	2.57	2.18	—	
AA800678	rc_AA800678_at	Similar to AW046014 protein (LOC363328)	2.03	2.00	—	
AA875523	rc_AA875523_s_at	Similar to 17 kDa myosin light chain (LOC362816)	2.04	2.00	—	
AA800803	rc_AA800803_g_at	EST190300 (Lung derived cDNA)	2.05	2.11	—	
VO↑ and PO→						
AI105348	rc_AI105348_i_at	Cofilin 1 (Cfl1)	2.20	1.13	actin binding	
M58404	M58404_at	Thymosin β-10 (testis-specific) gene	2.44	1.04	actin binding, actin monomer binding	

Table 1. (Continued)

Accession	Probe set ID	Gene name	VO	PO	Molecular function	Reference
AI180288	rc_AI180288_s_at	Caldesmon 1 (Cald1)	3.79	1.14	actin binding, calmodulin binding, myosin binding	
AA875132	rc_AA875132_at	Tropomyosin 1, α	2.36	0.95	actin binding, structural constituent of cytoskeleton	
AA893280	rc_AA893280_at	Adipose differentiation–related protein	2.01	0.82	adipocyte differentiation	
M23601	M23601_at	Monoamine oxidase B (Maobf3)	3.71	1.13	amine oxidase activity, oxidoreductase activity	
AA859829	rc_AA859829_g_at	Macrophage erythroblast attacher	2.08	0.96	apoptosis, cell adhesion, development	
S54008	S54008_i_at	Fibroblast growth factor receptor 1 β-isoform	2.22	1.12	ATP binding, fibroblast growth factor receptor activity	
AA875002	rc_AA875002_at	Leucine-rich repeat-containing 8 (LOC311846)	2.52	0.84	B cell development	
M83143	M83143_g_at	β-Galactoside-α 2,6-sialyltransferase	2.06	0.81	β-galactoside α-2,6-sialyltransferase activity	
U90121	U90121_at	Thrombomodulin	3.22	1.11	blood coagulation	
AF027984	AF027984_at	Low voltage-activated, T-type calcium channel α subunit	2.13	1.11	calcium channel activity, calcium ion binding	
AA891204	rc_AA891204_s_at	Secreted acidic cysteine rich glycoprotein (Sparc) or osteonectin	2.46	1.13	calcium ion binding	*22*
X06916	X06916_at	Protein p9Ka homologous to calcium-binding protein	2.14	0.85	calcium ion binding	
AA849769	rc_AA849769_at	Follistatin-related protein precursor or Follistatin-like (Fstl)	3.22	1.19	calcium ion binding, heparin binding	*21*
X51529	X51529_at	Platelet phospholipase A	3.79	0.85	calcium ion binding, phospholipase A2 activity	
X89963	X89963_at	Thrombospondin 4 (Thbs4)	4.41	0.93	calcium ion binding, structural molecule activity	
AI145680	rc_AI145680_s_at	Monocarboxylate transporter or Solute carrier family 16, member 1	2.17	1.14	carrier activity, monocarboxylate porter activity	
AB000778	AB000778_s_at	Phospholipase D	2.46	0.85	catalytic activity, hydrolase activity, phospholipase D activity	
X82396	X82396_at	Cathepsin B	2.12	1.12	cathepsin B activity, cysteine-type endopeptidase activity	
L03201	L03201_at	Cathepsin S	2.38	0.90	cathepsin S activity, cysteine-type endopeptidase activity	
AF020618	AF020618_g_at	Myeloid differentiation primary response gene 116	2.24	0.86	cell differentiation	
AA874848	rc_AA874848_s_at	Thy-1 gene for cell-surface glycoprotein	2.42	1.20	cell-cell interaction	
AA799803	rc_AA799803_at	Complement component 1, r subcomponent	2.36	0.96	chymotrypsin activity, trypsin activity	
M14656	M14656_at	Osteopontin	3.43	1.03	cytokine activity, growth factor activity, integrin binding	
X59864	X59864mRNA_g_at	ASM15 gene	2.98	1.15	cytoplasmic protein	
U16025	U16025_at	Class Ib RT1 or M3 protein (M3 gene)	2.82	1.18	defense response, immune response	
AI232374	rc_AI232374_g_at	H1 histone family, member 0 (H1f0)	2.07	1.19	DNA binding	
M31322	M31322_at	Sperm membrane protein (YWK-II)	2.20	1.19	DNA binding, endopeptidase inhibitor activity	
AA800613	rc_AA800613_at	Gene for TIS11 or Zinc finger protein 36 (Zfp36)	2.83	0.94	DNA binding, transcriptional activator activity	
M65149	M65149_at	CCAAT/enhancerbinding, protein (C/EBP) δ (Cebpd)	2.30	0.83	DNA binding, protein binding	
X60769	X60769mRNA_at	Interleukin-6-dependent binding protein	2.57	1.05	DNA binding, protein binding, transcriptional activator activity	
AA891041	rc_AA891041_at	Jun-B oncogene	3.21	0.93	DNA binding, transcription factor activity	
AB012231	AB012231_s_at	NF1-B2	2.11	1.11	DNA binding, transcription factor activity	
AA891717	rc_AA891717_at	Upstream transcription factor 1	2.32	1.19	DNA binding, transcription factor activity	
AA892520	rc_AA892520_g_at	Vesicle amine transport protein 1 homolog	2.27	0.99	DNA binding, zinc ion binding, oxidoreductase activity	
AF041066	AF041066_at	Ribonuclease 4	2.09	1.17	endonuclease activity, hydrolase activity, nuclease activity	
U42719	U42719_at	Complement component 4a	2.00	0.82	endopeptidase inhibitor activity	
J04035	J04035_at	Tropoelastin	2.54	1.17	extracellular matrix constituent conferring elasticity	

Table 1. (Continued)

Accession	Probe set ID	Gene name	VO	PO	Molecular function	Reference
U17834	U17834_at	Biglycan	2.66	1.16	extracellular matrix protein	
X84039	X84039_at	Lumican	2.10	1.03	extracellular matrix protein	
X17053	X17053mRNA_s_at	Immediate-early serum-responsive JE gene	2.15	0.81	G-protein–coupled receptor binding, chemokine activity	
X05834	X05834_at	Fibronectin gene 3′ end	2.46	0.82	heparin binding, mercury ion binding, oxidoreductase activity	
M36317	M36317_s_at	Thyrotropin-releasing hormone (TRH) precursor	3.34	0.86	hormone activity, thyrotropin-releasing hormone activity	
H31839	rc_H31839_at	BCL2-antagonist/killer 1 (Bak1)	2.17	0.94	induction of apoptosis	
AI233219	rc_AI233219_at	Endothelial cell-specific molecule 1	4.78	1.19	insulin-like growth factor binding	
AA894029	rc_AA894029_at	Endothelial type gp91-phox gene	3.03	1.09	ion channel activity, voltage-gated ion channel activity	
X16554	X16554_at	Phosphoribosylpyrophosphate synthetase subunit I	2.56	1.19	kinase activity, lipoate-protein ligase B activity	
U02553	U02553cds_s_at	Protein tyrosine phosphatase	2.74	1.19	MAP kinase phosphatase activity	
S74351	S74351_s_at	Protein tyrosine phosphatase	2.30	1.11	MAP kinase phosphatase activity	
S81478	S81478_s_at	Oxidative stress–inducible protein tyrosine phosphatase	2.20	0.84	MAP kinase phosphatase activity	
AI169327	rc_AI169327_at	Tissue inhibitor of metalloproteinase-1 (TIMP1)	2.32	1.19	metalloendopeptidase inhibitor activity	
X06801	X06801cds_i_at	Vascular α-actin	3.09	1.15	motor activity, structural constituent of cytoskeleton	*22*
L00088	L00088expanded_cds#2	Fast myosin alkali light chains	2.90	0.81	motor activity, structural constituent of muscle	
AA866276	rc_AA866276_at	Myeloid-associated differentiation marker	2.43	0.94	myeloid blood cell differentiation	
AA945737	rc_AA945737_at	Chemokine receptor LCR1	2.35	0.95	neuronal cell recognition	
U90610	U90610_at	CXC chemokine receptor (CXCR4)	2.18	1.11	neuronal cell recognition	
AA874999	rc_AA874999_at	Sec61 β subunit	2.11	1.14	protein targeting, protein transport	
U42627	U42627_at	Dual-specificity protein tyrosine phosphatase (rVH6)	2.58	1.18	protein tyrosine/serine/threonine phosphatase activity	
AA874889	rc_AA874889_g_at	Unc-5 homolog B	2.29	0.95	receptor activity, netrin receptor activity, protein binding	
X07636	X07636_at	Hepatic lectin	2.35	1.14	receptor activity, sugar binding	
M91590	M91590_at	β-Arrestin2	2.65	1.08	regulation of G-protein coupled receptor protein signaling	
AI008423	rc_AI008423_at	Unc-50 related protein (UNCL)	2.01	1.19	RNA binding	
AA860043	rc_AA860043_at	Guanine nucleotide binding protein γ subunit 11 (Gng11)	2.26	1.03	signal transducer activity	
AA894345	rc_AA894345_at	Phosphoprotein enriched in astrocytes 15	2.17	0.85	sugar porter activity, protein binding	
AA893235	rc_AA893235_at	Similar to G0S2-like protein	2.60	0.96	—	
X52815	X52815cds_f_at	Similar to γ actin–like protein	2.01	1.17	—	
AA892391	rc_AA892391_at	Similar to hypothetical protein FLJ20531 (LOC303164)	3.85	1.16	—	
AA893267	rc_AA893267_at	Similar to proline-serine-threonine phosphatase–interacting protein 1	2.06	0.84	—	
AA799571	rc_AA799571_at	Similar to RIKEN cDNA 1110001M20 (LOC298308)	2.01	1.19	—	
AA892578	rc_AA892578_at	Similar to RIKEN cDNA 6330406I15 (LOC360757)	2.83	1.00	—	
AA891940	rc_AA891940_at	Similar to transforming protein RhoC (H9)	2.36	0.91	—	
AA892333	rc_AA892333_at	Similar to tubulin α-6	2.13	0.81	—	*20*
AA891690	rc_AA891690_g_at	Similar to tumor necrosis factor ligand superfamily member 13	2.37	1.07	—	
AA894292	rc_AA894292_at	EST198095 (Spleen derived cDNA)	2.31	0.87	—	
AA894092	rc_AA894092_at	EST197895 (Spleen derived cDNA)	4.98	1.14	—	
AA891677	rc_AA891677_at	EST195480 (kidney derived cDNA)	2.07	1.14	—	

Table 1. (Continued)

Accession	Probe set ID	Gene name	VO	PO	Molecular function	Reference
VO↑ and PO↓						
J02780	J02780_at	Tropomyosin 4 (Tpm4)	2.70	0.48	actin binding	*19*
M34043	M34043_at	Thymosin β-4 (pTB4G)	2.32	0.49	actin binding	*19*
M83107	M83107_at	Transgelin (Smooth muscle 22 protein) (Tagln)	2.28	0.44	actin filament binding, protein binding, bridging	
L12380	L12380_at	ADP-ribosylation factor 1 (Arf1)	2.95	0.40	GTP binding, GTPase activity, protein transporter activity	
X74402	X74402_at	Guanosine diphosphate dissociation inhibitor 1 (Gdi1)	2.45	0.47	GTPase activator activity, RAB GDP-dissociation inhibitor activity	
D30740	D30740_at	14-3-3 protein mRNA for mitochondrial import stimulation factor S1	2.36	0.44	monooxygenase activity, protein domain specific binding	
AA799520	rc_AA799520_at	Integral membrane protein 2B	2.00	0.43	neurogenesis	*21*
X76489	X76489cds_g_at	CD9 mRNA for cell surface glycoprotein	2.37	0.33	protein binding	
AA875033	rc_AA875033_at	Fibulin 5 (Fbln5)	2.16	0.49	regulation of cell growth	*19*
AA850734	rc_AA850734_at	Vascular endothelial growth factor A (Vegfa)	2.12	0.49	vascular endothelial growth factor receptor binding	
AA875537	rc_AA875537_at	Similar to splicing factor arginine/serine rich 2 (SC-38)	2.55	0.32	—	
VO→ and PO↑						
M60655	M60655_at	α-1B adrenergic receptor	1.03	2.05	α1-adrenergic receptor activity	
AI639058	rc_AI639058_s_at	Transmembrane, prostate androgen induced RNA	1.17	2.19	androgen receptor signaling pathway	
AF014009	AF014009_at	Acidic calcium-independent phospholipase A2	0.80	2.02	antioxidant activity, catalytic activity, hydrolase activity	*21*
M22631	M22631_at	α-Propionyl-CoA carboxylase	1.14	2.02	ATP binding, biotin binding, propionyl-CoA carboxylase activity	
U10357	U10357_at	Pyruvate dehydrogenase kinase 2 subunit p45	1.19	2.30	ATP binding, pyruvate dehydrogenase kinase activity	
X75253	X75253_at	Phosphatidylethanolamine binding protein (Pbp)	0.83	2.00	ATP binding, serine-type endopeptidase inhibitor activity	
D86039	D86039_at	Potassium inwardly rectifying channel, subfamily J, member 11	0.98	2.18	ATP-activated inward rectifier potassium channel activity	
AI169417	rc_AI169417_s_at	Phosphoglycerate mutase type B subunit	1.12	3.61	bisphosphoglycerate phosphatase activity, catalytic activity	
M86621	M86621_at	Dihydropyridine-sesitive L-type calcium channelα-2 subunit	1.02	2.18	calcium channel activity, ion channel activity	
AA892511	rc_AA892511_at	Tescalcin	0.92	2.07	calcium ion binding	
AA892146	rc_AA892146_f_at	Similar to carboxypeptidase B gene	1.13	2.02	carboxypeptidase activity, metallopeptidase activity	
X66494	X66494_at	Choline transporter (CHOT1)	0.91	2.00	choline transporter activity, creatine transporter activity	
AB012234	AB012234_g_at	Nuclear factor I/X (Nfix)	1.11	2.01	DNA binding, transcription factor activity	
U17837	U17837UTR#1_g_at	Zinc finger protein RIZ	0.86	2.06	DNA binding transcription factor	*19*
AA899106	rc_AA899106_at	G1/S-specific cyclin D2 (VIN-1 proto-oncogene) (LOC297611)	1.14	2.19	G1/S transition of mitotic cell cycle, cell growth	
AA799788	rc_AA799788_s_at	Cell division cycle 34	0.99	2.10	G2 checkpoint	
AA799570	rc_AA799570_at	DnaJ (Hsp40) homolog, subfamily A, member 4	1.11	2.02	heat shock protein binding, unfolded protein binding	*19*
M33962	M33962_g_at	Protein-tyrosine-phospatase	0.93	2.02	hydrolase activity, phosphoprotein phosphatase activity	
AJ006971	AJ006971_g_at	Death-associated like kinase (Dapk)	0.80	2.08	induction of apoptosis	
AI043968	rc_AI043968_at	Caveolin-3	1.03	2.00	integral to membrane	
AA859981	rc_AA859981_at	Similar to myo-inositol monophosphatase 2 (Impa2)	0.82	2.02	magnesium ion binding, inositol-1(or 4)-monophosphatase activity	

Table 1. (Continued)

Accession	Probe set ID	Gene name	VO	PO	Molecular function	Reference
X53054	X53054_at	RT1.D β chain	0.99	2.16	MHC class II protein	
AI227608	rc_AI227608_s_at	Microtubule-associated protein tau (Mapt)	1.16	2.02	microtubule-based process	
U59126	U59126_at	TR4-NS orphan receptor (TR4) gene	1.13	5.34	nuclear hormone receptor	
AF077354	AF077354_at	Ischemia responsive 94 kDa protein (irp94)	1.00	2.20	response to heat	
M29293	M29293_at	Small nuclear ribonucleoparticle-associated protein (snRNP)	1.12	2.03	RNA binding, pre-mRNA splicing factor activity	
U82224	U82224_at	Cardiac titin N2B isoform (Ttn)	1.15	3.79	sarcomere organization	
X78985	X78985cds_s_at	CD5 or Hocyte antigen CD5	0.81	4.28	scavenger receptor activity	
AA892843	rc_AA892843_at	Mitochondrial ribosomal protein L24	1.06	2.04	structural constituent of ribosome	
X56228	X56228_g_at	Rhodanese or thiosulfate sulfurtransferase (Tst)	0.80	2.31	thiosulfate sulfurtransferase activity, transferase activity	
AA858586	rc_AA858586_at	Suppressor of Ty 5 homolog (*S. cerevisiae*) (Supt5h)	1.14	2.16	transcription elongation factor activity	
M62752	M62752_at	Statin-related protein (S1) gene	0.87	2.10	translation elongation factor activity, GTP binding	
AA892507	rc_AA892507_at	Immature colon carcinoma transcript 1	1.12	2.00	translation release factor activity	
AA799691	rc_AA799691_at	K-Cl cotransporter KCC4	1.01	2.00	transport, ion transport, potassium ion transport	
AA799475	rc_AA799475_at	Ankyrin repeat domain 24	0.88	2.05	—	
AA875261	rc_AA875261_at	CSX-associated LIM	1.17	2.08	—	
AA893821	rc_AA893821_at	P34 protein	1.19	2.12	—	
AA892005	rc_AA892005_at	SCIRP10-related protein	1.02	2.08	—	
AA891802	rc_AA891802_at	Similar to cysteine and histidine rich 1	1.16	2.04	—	
AA800039	rc_AA800039_s_at	Similar to hypothetical protein MGC6696 (LOC293719)	1.02	2.12	—	
AA799766	rc_AA799766_at	Similar to Jtv1-pending protein	0.92	2.00	—	
AA892768	rc_AA892768_at	Similar to putative breast adenocarcinoma marker (32 kDa)	1.19	2.30	—	
AA799654	rc_AA799654_g_at	Similar to WD repeat-containing F-box protein FBW5	1.02	2.12	—	
AA866454	rc_AA866454_at	Similar to α-2(I) promoter	1.16	2.00	—	
AA892773	rc_AA892773_at	EST196576 (kidney derived cDNA)	1.02	2.02	—	
AA891631	rc_AA891631_at	EST195434 (kidney derived cDNA)	0.93	2.02	—	
AA799932	rc_AA799932_at	EST189429 (heart derived cDNA)	1.09	2.09	—	
VO→ and PO↓						
U93306	U93306_at	VEGF receptor-2/FLK-1	1.01	0.49	ATP binding, kinase activity, protein kinase activity	
X53363	X53363cds_s_at	Calreticulin (Calr)	0.82	0.36	calcium ion binding, calcium ion storage activity	
AF047707	AF047707_at	UDP-glucose:ceramide glycosyltransferase	1.13	0.45	ceramide glucosyltransferase activity	
U95727	U95727_at	DnaJ (Hsp40) homolog, subfamily A, member 2 (Dnaja2)	0.89	0.45	chaperone activity	*19*
X16043	X16043cds_at	Phosphatase 2A catalytic subunit isotype α	0.92	0.47	CTD phosphatase activity, calcium-dependent phosphatase activity	
D17711	D17711cds_s_at	Heterogeneous nuclear ribonucleoprotein K (Hnrpk)	1.13	0.32	DNA binding, RNA binding, nucleic acid binding	
AA799582	rc_AA799582_at	Heterogeneous nuclear ribonucleoprotein K (Hnrpk)	1.17	0.48	DNA binding, RNA binding, nucleic acid binding	
U53922	U53922_at	DnaJ-like protein (RDJ1)	0.82	0.47	DNA damage response, perception of DNA damage	
D21800	D21800_at	Proteasome subunit RC10-II	0.83	0.43	endopeptidase activity, hydrolase activity, peptidase activity	

Table 1. (Continued)

Accession	Probe set ID	Gene name	VO	PO	Molecular function	Reference
AF072411	AF072411_g_at	Fatty acid translocase/CD36	1.13	0.35	fatty acid binding, receptor activity	
S81353	S81353_s_at	Sulfated glycoprotein-1 or Prosaposin (Psap)	0.89	0.25	glycolipid transport, sphingolipid metabolism	
M83676	M83676_at	Similar to RAB12, member RAS oncogene family (Rab12)	0.92	0.49	GTP binding, protein transporter activity	
D84477	D84477_at	Plysia ras-related homolog A2 (Arha2)	1.19	0.25	GTPase activity, GTP binding	
X68101	X68101_at	Dedicator of cytokinesis 9	1.16	0.46	guanyl-nucleotide exchange factor activity, GTP binding	
AF000942	AF000942_at	Inhibitor of DNA binding 3	1.11	0.43	inhibitor of transcription	
M19533	M19533mRNA_i_at	Cyclophilin or peptidylprolyl isomerase A (Ppia)	0.88	0.46	isomerase activity, peptidyl-prolyl *cis-trans* isomerase activity	
AI102620	rc_AI102620_at	Mitogen activated protein kinase kinase kinase 1	0.95	0.47	magnesium ion binding, protein kinase activity	
AI011706	rc_AI011706_at	Splicing factor, arginine/serine-rich 3 (SRp20)	0.99	0.49	nucleic acid binding, RNA binding	
D84346	D84346_s_at	NCK-associated protein 1 (Nap1) protein or Hem-2	0.88	0.21	protein binding	
D78303	D78303_at	YT521 for RNA splicing-related protein	1.09	0.49	protein binding	
AA891035	rc_AA891035_at	Beclin 1 (coiled-coil, myosin-like BCL2-interacting)	1.11	0.45	protein binding	
S59892	S59892_f_at	La=autoantigen SS-B/La (3′ region, clone K4)	0.89	0.43	RNA binding, nucleic acid binding	
AF030091	AF030091UTR#1_g_at	Cyclin ania-6a	1.10	0.49	RNA processing	
AB022209	AB022209_s_at	Ribonucleoprotein F	1.18	0.46	TATA-binding protein binding, pre-mRNA splicing factor activity	
AF048687	AF048687_s_at	UDP-Gal:glucosylceramide β-1,4-galactosyltransferase	1.18	0.45	UDP-galactose-glucosylceramide galactosyltransferase activity	
AF034237	AF034237_s_at	DD6A4-1	1.13	0.49	—	
U64705	U64705cds_i_at	Eukaryotic translation initiation factor 4A2	0.89	0.49	—	
AA891535	rc_AA891535_at	Hippocampus abundant gene transcript 1	1.18	0.49	—	
AA892376	rc_AA892376_at	Protein associated with PRK1	1.19	0.44	—	
AA892918	rc_AA892918_at	Similar to tight junction protein 1 (Tjp1)	1.19	0.47	—	
VO↓ and PO↑						
L22294	L22294_at	Pyruvate dehydrogenase kinase-1 (Pdk1)	0.44	2.02	ATP binding, pyruvate dehydrogenase kinase activity	*19*
D10754	D10754_at	Proteasome subunit R-DELTA	0.48	2.19	endopeptidase activity, hydrolase activity, peptidase activity	
X62660	X62660mRNA_at	Glutathione transferase subunit 8	0.46	2.06	—	
AA891037	rc_AA891037_g_at	Similar to 60S ribosomal protein L3-like	0.47	2.05	—	
AA799888	rc_AA799888_at	Similar to mitochondrial ribosomal protein L40	0.49	2.00	—	
VO↓ and PO→						
D16478	D16478_at	Hydroxyacyl-CoA dehydrogenase/3-ketoacyl-CoA hiolase/enoyl-CoA hydratase α subunit	0.49	0.92	3-hydroxyacyl-CoA dehydrogenase activity	
D00512	D00512_at	Mitochondrial acetoacetyl-CoA thiolase	0.43	0.98	acetyl-CoA C-acetyltransferase activity, acyltransferase activity	
J02752	J02752_at	Acyl-coA oxidase	0.48	0.83	acyl-CoA oxidase activity	
M60322	M60322_g_at	Aldehyde reductase 1 (low Km aldose reductase) (Aldr1)	0.49	1.08	aldehyde reductase activity, oxidoreductase activity	
M21060	M21060_s_at	Copper-zinc containing superoxide dismutase	0.46	1.05	antioxidant activity, copper, zinc superoxide dismutase activity	
AI104924	rc_AI104924_f_at	α-Cardiac myosin heavy chain	0.48	1.06	ATP binding, actin binding, calmodulin binding, motor activity	
AA800190	rc_AA800190_g_at	Brain glycogen phosphorylase (Pygb)	0.43	0.89	catalytic activity, glycogen phosphorylase activity	